

https://dspace.org/

Investigating the effect of gold-palladium bimetallic nanoparticles on TiO2 and the catalytic activity in CO oxidation

Ntholeng, Nthabiseng

2013-04-29
http://hdl.handle.net/10539/12693

Downloaded from a DSpace repository. https://dspace.org/

Chapter 3

Synthesis of supported gold catalysts via deposition precipitation (DP) method

3.1 Introduction

Deposition precipitation (DP) method is by far the mostly recommended method for synthesizing small sized gold particles [1]. However, this method requires careful control, with pH of the solution being particularly the most important factor during synthesis. The pH at which gold is precipitated is important for growth and nucleation of gold particles [2]. Hence it is determined according to the isoelectric point (IEP) of the metal oxide support [3].The IEP of the support changes the positions of the active sites of precipitation and this is related to the pH of the solution. The pH below the isoeletric point of the support will result in a positively charged surface which facilitates adsorption of negatively charged gold species. Hence there will be larger gold loading and high concentration of chloride ions present on the support that increases mobility of Au particles leading to formation of large gold particles. At a pH above the isoeletric point there is a rapid decrease of adsorption of negatively charged $Au(OH)_x(Cl)_{4-x}^-$ complex resulting in low gold loading [4-5].

The equilibrium constants measured by Nechayev and Nikolenko (Fig 3.1) shows different types of species present at a particular pH [6]. At pH 3-4 the major species are neutral $AuCl_3.H_2O$, and at pH 7 which is mostly preferred for the DP method, $[AuCl(OH)]_3^-$ is predominant. At pH 10 and above, the $[Au(OH)]_4^-$ anion is the dominant species. The isoelectric point of P-25 TiO_2 is reported to be in the range of 4.5–6.3, so that anionic species should adsorb by electrostatic attraction at lower pH; neutral species, of course, will not adsorb in this manner [7-8]. There are three processes that occur when pH is varied during the mixing of the gold solution. During hydrolysis of $[AuCl_4]^-$ neutral species are produced by displacing Cl^- ions (reaction 1-3), loss of protons from the neutral species(reaction 2 and 4) and Cl^- ions are replaced by OH^- ions during hydrolysis (reaction 5 and 6) [9].

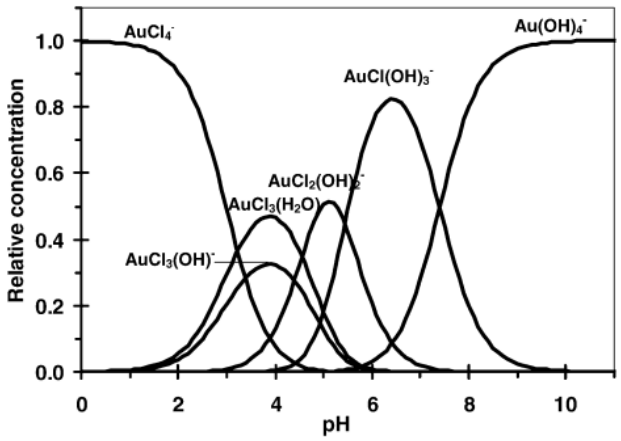

Figure 3.1. Relative equilibrium concentration of gold complexes ([Cl^-] =2.5 × 10^{-3}M) as a function of the pH of the solution, calculated with equilibrium constants reported by Nechayev et al. [5]

$$[AuCl_4]^- + H_2O \leftrightarrow AuCl_3(H_2O) + Cl^- \quad [1]$$

$$AuCl_3(H_2O) \leftrightarrow [AuCl_3(OH)]^- + H^+ \quad [2]$$

$$[AuCl_3(OH)]^- + H_2O \leftrightarrow AuCl_2(H_2O)(OH) + Cl^- \quad [3]$$

$$AuCl_2(H_2O)(OH) \leftrightarrow [AuCl_2(OH)_2] + H^+ \quad [4]$$

$$[AuCl_2(OH)_2]^- + H_2O \leftrightarrow [AuCl(OH)_3]^- + Cl^- + H^+ \quad [5]$$

$$[AuCl(OH)_3]^- + H_2O \leftrightarrow [Au(OH)_4]^- + Cl^- + H^+ \quad [6]$$

Therefore, there is a narrow range of pH where small sized Au particles can be adsorbed on the support with minimal chloride in the Au complex. Lee and Graviilidis reported that for Au/γ -Al_2O_3, increasing the pH of the solution up to pH 7 increases the concentration of strongly adsorbing complexes ($AuCl_2(OH)_2$ and $AuCl(OH)_3$ and therefore the optimum value of pH is expected where the concentration of the strongly adsorbed species is maximized. Moreau et al reported the optimum pH for highly active Au/TiO_2 catalysts to be 9 [9]. Li et al. showed that for a series of catalysts prepared by DP method, activity increased with increasing pH but there was a rapid decrease in activity at pH of 11 [10]. Wolf and Schüth confirmed the optimum pH of 10 [11].

The precipitating pH is not only the vital parameter which should be monitored during synthesis, there are a few other parameters to be controlled. A successful synthesis of supported gold catalysts via DP will require a careful control of the following parameters: (i) the concentration of the $HAuCl_4$ solution; (ii) the ratio of $HAuCl_4$ solution volume and

concentration to the mass of support; (iii) the type of TiO_2 (Degussa P-25 is the most commonly chosen); (iv) the base chosen to neutralise the $HAuCl_4$ solution; (v) the temperature at which this is done; (vi) the pH, (vii) the time and then temperature allowed for the deposition to occur; (viii) the method of filtration, washing, and drying; (ix) the conditions for calcination (if performed). However, literature reports an incomplete picture of the optimum procedure that should be adopted to secure high activity for carbon monoxide oxidation. This study seeks to investigate effects of pH, calcinations temperature, gold loadings and aging on particle size in order to determine the optimum synthesis conditions of Au/TiO_2 catalysts. The effect of support on particle size will be investigated.

3.2 Catalyst synthesis

All the reagents used for synthesis of Au catalysts were commercially available and used without further purification. To study the effects of Au weight percentage (wt %), the following conditions were used as standard preparation conditions: pH 9, calcination temperature 200 ºC and aged for 72 h. The above conditions were chosen as standard conditions because pH 9 is easier to maintain and at 200 ºC the Au particles are said to be fully metallic as reported by Zanella et al. [12]. During synthesis the support (P25 TiO_2) was initially dissolved in de-ionized water and heated up to 70 ºC. The initial pH was raised to 9 prior precipitating the dissolved Au precursor. The dissolved Au solution was added dropwise while maintaining pH with NH_4OH solution. The synthesis was carried out for 2 h. The slurry was then cooled down to room temperature for 2 h while stirred. Furthermore, the slurry was closed with parafilm and stored in a dark cupboard for 72 h. The material was recovered by filtration and washed several times with distilled water. Thereafter the wet samples were dried in an oven for 2 h and calcined in air at the desired temperature for 2 h. There was a colour change observed upon heating from white to purple. To investigate the effects of pH, calcination temperatures, Au wt% , aging, and support on the particle size and activity of Au catalyst the above procedure from Raphulu et al. was adopted [13].

3.3 Catalyst characterization

3.3.1 The effect of Au content on particle size

The morphology of the prepared catalysts was observed with TEM. TEM images obtained (Fig 3.2) show Au metal adsorbed on the support as black tiny spots indicated by arrows. There seem to be hemispherical attached Au particles indicated by letter ***a***, and spherically buried Au particles in the support shown by letter ***b*** (Fig 3.2). The hemispherical adsorbed Au species suggests strong metal-support interaction. The lumpy black particles observed on the support indicated by letter ***x***, suggest the presence of chlorine contaminants resulting from poor control of pH, which favoured adsorption of negatively charged $Au(OH)_xCl_{4-x}^-$ complex. ICP analysis indicates that the actual Au loading was lower than the intended (nominal) loading (Table 3.1), suggesting that some of the Au could have been washed off or remained in the filtrate during filtration process hence an incomplete transport of Au to the support. This is particularly observed for catalysts with 0.05% actual metal loading (Fig 3.2a) where there are few Au particles visible on the support surface. This is in contrast to the findings of Moreau et al. where a high Au dispersion at 1% loading was attained [12]. It is observed that as Au loading increases, there is a uniform Au dispersion on the support indicating a strong metal-support interaction. The average particle size distribution obtained from TEM after measuring the diameter of more than 100 particles shows an increasing trend in particle size as the Au loading increases. In contrast to this, a catalyst with the lowest loading (0.05%) seems to have large Au particles of 5 nm in size according to the obtained size distribution (Fig 3.2b). This may be attributed to lack of pH control during synthesis that may have lead to adsorption of negatively charged species, hence causing large Au particles to form on the support. The 2.45% catalyst has average particle size of 3.5 nm while 7.79% and 9.89% seem to have the same mean particle size of 5.5 nm. Based on the calculated percentage error from the BET results (Table 3.1) it can be said that the measured particle size from the TEM results of 7.79% catalyst is more accurate than that of 9.89% catalyst as the is less % error.

For catalysts with 9.89% loading it could be most of the hydroxyl ions were consumed during precipitation, encouraging formation of smaller particles. Hence there was high dispersion of small sized Au particles compared to 7.79% which has low loaded Au content. It can therefore be concluded that the optimum Au loading in this study was 3% with a mean particle size of 3.5 nm. It is evident from these results that as more Au is deposited, under

these conditions, the bigger the particle size. The large particles size indicates weak metal-support interaction that leads to non-uniform dispersion of spherically adsorbed particles.

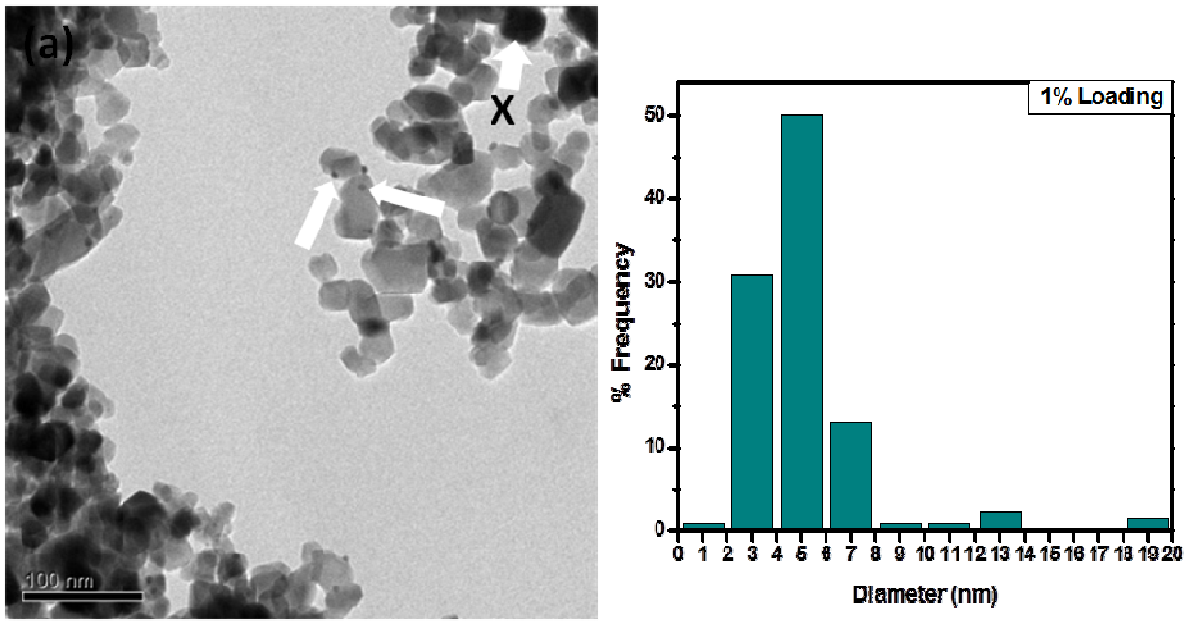

Figure 3.2a: TEM images and average particles size distribution of Au/TiO_2 catalysts with 1% gold loading. Good dispersion of small sized particles can be seen. The arrows indicate the dark spots that correspond to the loaded gold. The particle size distribution was obtained by counting more than 100 particles and determining their size.

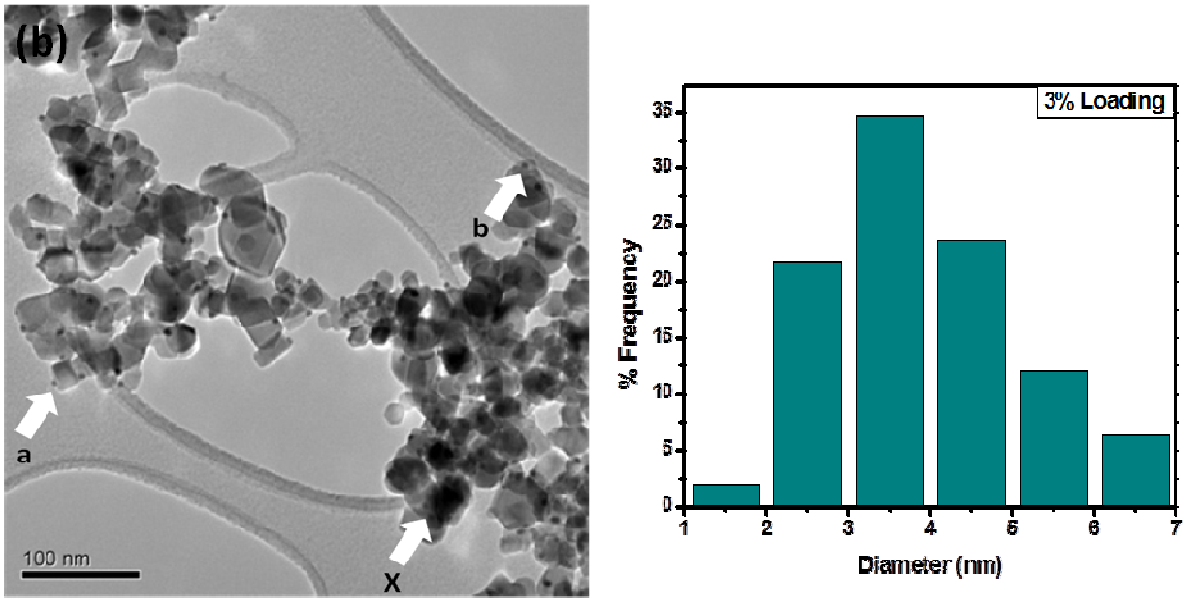

Figure 3.2b: TEM image and average particle size distribution of Au/TiO_2 catalyst with 3% gold loading. Good dispersion of hemispherical and spherical particles can be seen indicated by letter ***a*** and ***b*** respectively. The dark tiny spots indicated by letter X corresponds to gold loaded. The particle size distribution was obtained by counting more than 100 particles and determining their size.

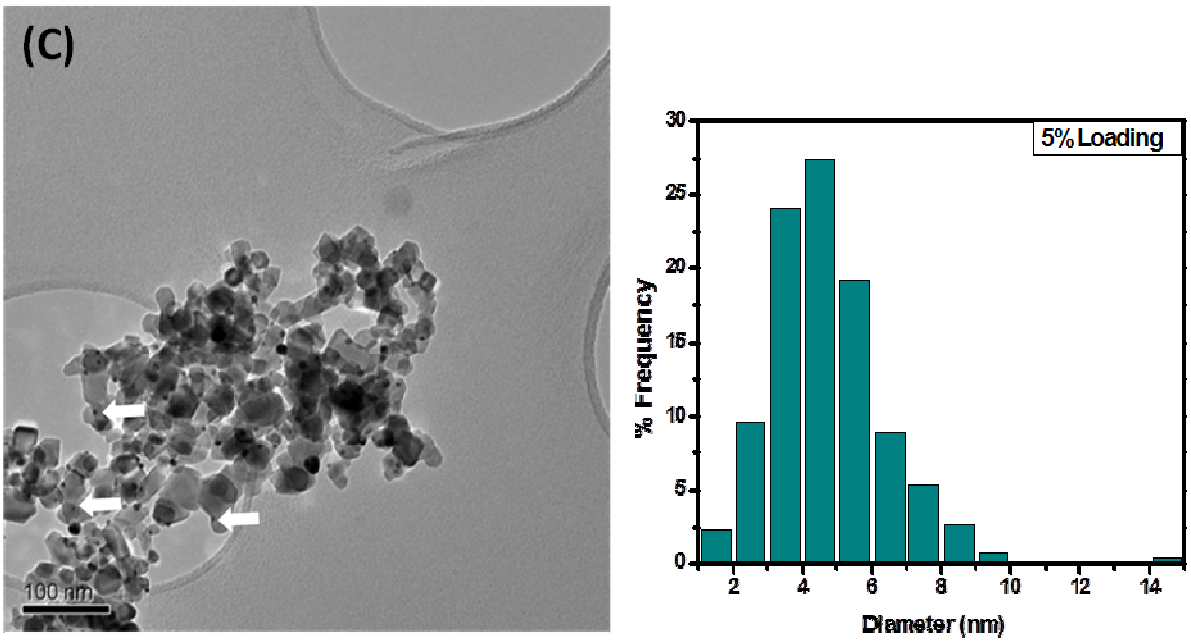

Figure 3.2c: TEM image and average particle size distribution of Au/TiO_2 catalyst 5% (nomial metal loading) gold loading. Good dispersion of hemispherical and spherical particles can be seen. The gold loaded is indicated by arrows. The particle size distribution was obtained by counting more than 100 particles and determining their size.

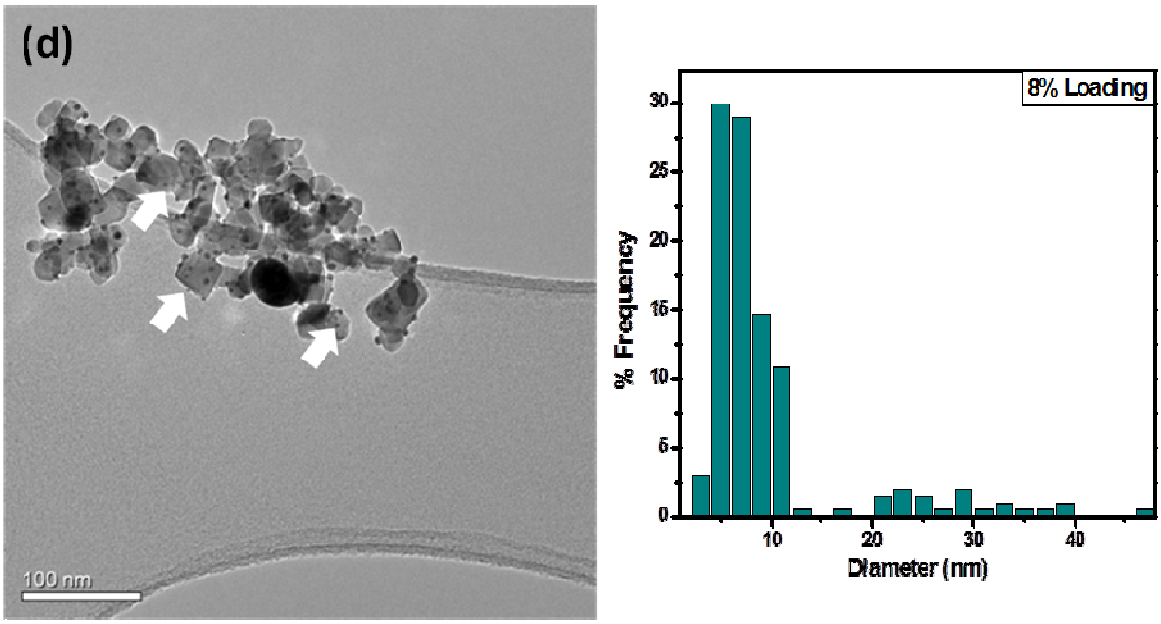

Figure 3.2d: TEM image and average particle size distribution of Au/TiO_2 catalyst 8% (nomial metal loading) gold loading. Good dispersion of hemispherical and spherical particles can be seen. The gold loaded is indicated by arrows. The particle size distribution was obtained by counting more than 100 particles and determining their size.

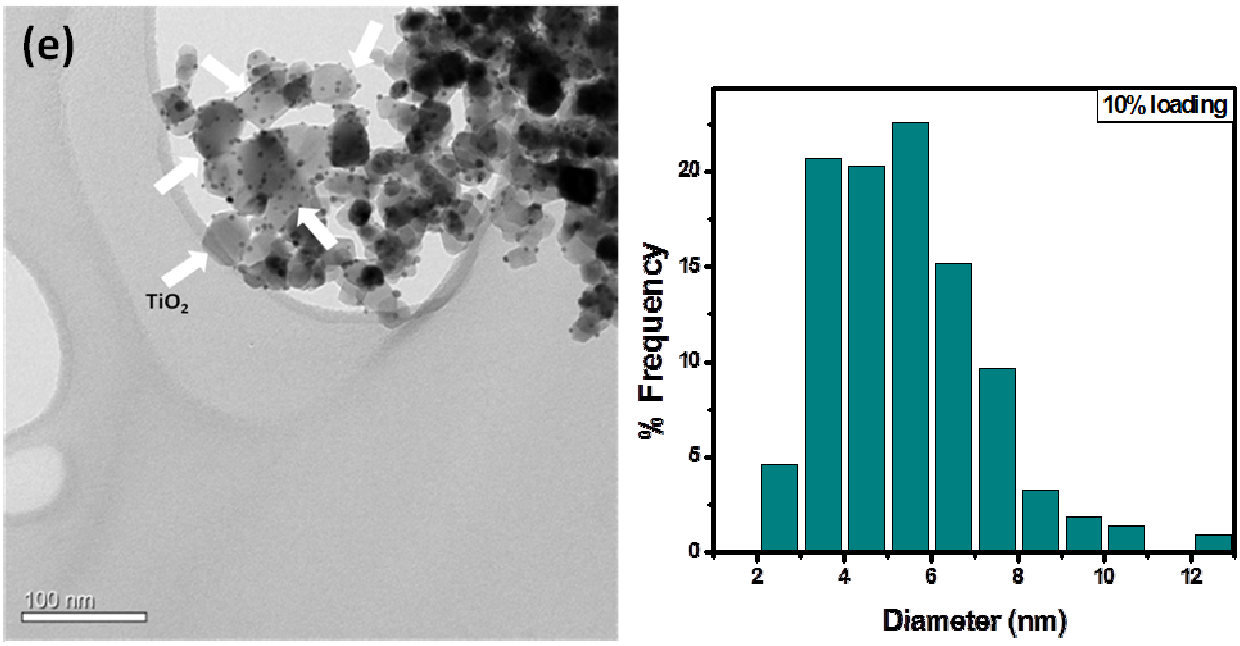

Figure 3.2e: TEM image and average particle size distribution of Au/TiO_2 catalyst 10% (nomial metal loading) gold loading. Good dispersion of hemispherical and spherical particles can be seen. The gold loaded is indicated by arrows. The particle size distribution was obtained by counting more than 100 particles and determining their size.

Table 3.1: Properties of prepared catalysts of various Au wt% showing the experimentally determined surface areas (S_{BET}) and average particle size after DP at pH 9.

Au wt.% Loading					
Actual Loading	**Theoretical Loading**	**S_{BET} ($m^2 g^{-1}$)**	**Pore Volume ($cm^3.g^{-1}$)**	**Particle size[a] (nm)**	**Particle size[b] (nm)**
0.05 Au/TiO_2	1 Au/TiO_2	44.29 (3.6) [c]	0.4153	5.5	5.3
2.45 Au/TiO_2	3 Au/TiO_2	46.09(7.8) [c]	0.4397	3.5	3.7
4.53 Au/TiO_2	5 Au/TiO_2	45.74(7.1) [c]	0.4008	4.5	3.6
7.79 Au/TiO_2	8 Au/TiO_2	43.01(0.6) [c]	0.3076	5.5	2.3
9.89 Au/TiO_2	10 Au/TiO_2	37.73(11) [c]	0.2986	5.5	2.3
P25(TiO_2)	-	42.72	0.1526	-	-

[a] TEM [b] XRD [c] % Error

The surface area of the prepared catalysts was determined by measurement of the amount of N_2 physically adsorbed as a function of pressure. The obtained results (Table 3.1) show that the P25 degussa TiO_2 (74% anatase and 26% rutile) support had the surface area of $42.7 m^2 g^{-1}$ which changed upon deposition of Au particles. It was observed that as the Au content increases there was a decrease in surface area. This seems to suggest a high deposition of Au

particles on the pores. A decrease in pore volume could be attributed to pores blocked by Au particles. It is observed from the Table 3.1 that the pore volume of the 0.05% catalysts is small compared to 5% catalysts. For catalysts with high Au loading from 5% to 10% there was a decrease in pore volume from 0.400 $cm^3.g^{-1}$ to 0.298 $cm^3.g^{-1}$. This confirms the TEM results showing that the precipitated Au particles have large particles size. However, there was no significant decrease observed in pore volume for catalysts with 7.79% and 9.89% Au loading, and that is in agreement with the obtained particle size from TEM.

PXRD technique was also employed to monitor the crystallinity of both the support and metal particles. The diffraction patterns were recorded from 2θ = 40º to 50°. It was observed that when the scan range was from 10º to 60º 2θ the two major Au peaks reported by Maciejewski et al. at 2θ = 38.2° and 44.4° due to Au (111) and Au (200) respectively were not detectable [14]. The peak at 2θ = 38.2° overlapped with the Ti (004) peak. In this study particle size was determined from the Au (200) peak observed at 44.4° 2θ. Other observed peaks are to those from anatase and rutile, characteristic of Degussa P25 [15]. The obtained diffraction pattern (Fig.3.3) shows a prominent Au peak at 44.4° 2θ. It is observed that the Au (200) peak grows broader as the wt% increases indicating a decrease in particle size. The average crystal size is summarized in Table 3.1. Catalyst with 10% loading (theoretical loading) seems to have a shoulder at 44.4° 2θ that may have resulted from a change in lattice structure occured during XRD measurements. The average crystal size estimated from line broadening analysis shows formation of small Au particles on the support which is consistent with the obtained TEM results. The obtained average crystallite size maybe attributed to overlapping peaks [16].

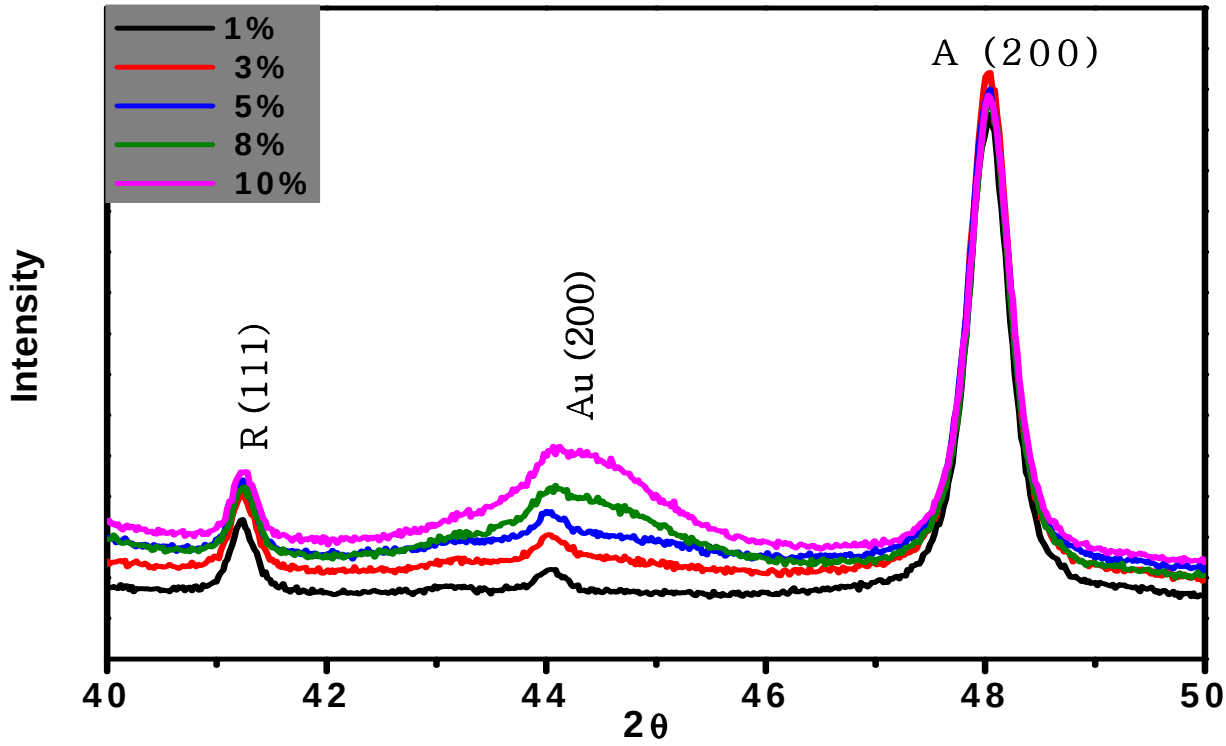

Figure 3.3: XRD patterns of Au/TiO_2 catalysts with various Au loading with R and A indicating diffraction peaks for rutile and anatase respectively.

3.3.2 The effect of pH on particle

The DP method used was slightly different from the one described by Haruta in the literature [17]. The described DP procedure by Haruta entails addition of the support material to the Au solution. The synthesis carried out involved dissolving the support in the deionized water at 70 °C prior to addition of $HAuCl_4$ solution. The initial pH was 2.6, and was raised to various values (7.5-10) by adding NH_4OH solution. However, maintaining constant pH was difficult, particularly for pH 7 that is the most preferred pH for the DP method. The observed decrease in pH during synthesis indicated that there was a slow consumption of OH^- anions suggesting that both hydrolysis of the different anions and their ligand exchange are slow, hence preparation lasted more than 1 h. As a result there was an insignificant difference observed between the actual and nominal gold loading (Table 3.2) indicating significant deposition of Au particles on the support. The fall in Au content could be accounted for by an electrostatic repulsion of gold-containing anions on the negatively charged surface of the support. The negatively charged surface usually occurs at pH above the isoeletric point which in this case is at pH above 6.

Table 3.2: Properties of prepared catalysts with 3% metal loading (theoretical loading) showing experimentally determined surface areas (S_{BET}) and average particle size after DP at various pH.

Actual Loading	pH	S_{BET} ($m^2 g^{-1}$)	Pore Volume ($cm^3.g^{-1}$)	Particle size[a] (nm)	Particle size[b] (nm)
2.45 Au/TiO_2	7.5	38.88(8.9)[c]	0.3570	4.3	3.6
2.89 Au/TiO_2	8	44.07(3.1)[c]	0.3351	3.7	5.3
2.53 Au/TiO_2	9	44.10(3.2)[c]	0.3305	3.5	4.7
2.93 Au/TiO_2	10	36.44(4.7)[c]	0.3236	3.3	4.3

[a] TEM [b] XRD [c] % Error

TEM images show that, as the pH increases there is high dispersion of small sized Au particles (Fig.3.4) adsorbed on the support. It was also observed that there was existence of a mixture of sizes that could be attributed to driving force for Ostwald ripening [18]. This driving force does not exist when the particles are uniformly small [19]. The non-uniform pH across the solution might have triggered regions with more rapid gold deposition (small particles) and regions with slow gold DP, hence larger particles. The average particles size is shown in histograms (Fig.3.4) plotted after measuring the diameter of more than 100 Au particles. The graphs show that as pH increases the size decreases, with pH 10 showing the smallest Au particles of 3.3 nm in size. However, the obtained curve for particle size distribution of pH 10 and pH 9 showed frequency distribution of mean particle size, that does not follow a bell curve. Therefore it can be said that pH 8 is the optimum, since the particle size distribution curve follows normal distribution, which is statically correct for approximating a sum of large number of random values which cluster around a single mean value. However, through analysis of the number of Au particles on the support is required.

According to BET results (Table 3.2) pH 7.5 and pH 10 has the lowest surface area of 38.8 m^2g^{-1} and 36.4 m^2g^{-1} respectively, suggesting the presence of large Au particles deposited on the surface of the support. For pH 8 and 9 there was an increase in the surface area, showing good dispersion of uniform Au particles on the support. In contrary to TEM results, pH 10 has the lowest surface area of 36.4 m^2g^{-1} suggesting dispersion of large particles onto the support.

The XRD patterns (Fig.3.5) show a decrease in the Au (200) peak area indicating a decrease in particle size. The observed trend on XRD results agrees with the literature showing that at high pH more and more small sized Au particles are dispersed on the support. The small sized Au particles also suggest less adsorption of chlorine contaminants on the supports which is thought to facilitate particle sintering [10]. Hence the XRD results are in agreement

with the obtained TEM results, although obtained values are not equal. The large crystal size obtained from XRD results could be attributed to short scan range which was measured over a long period of time, as such there is a possibility that x-ray radiation might have caused particle sintering during measurements.

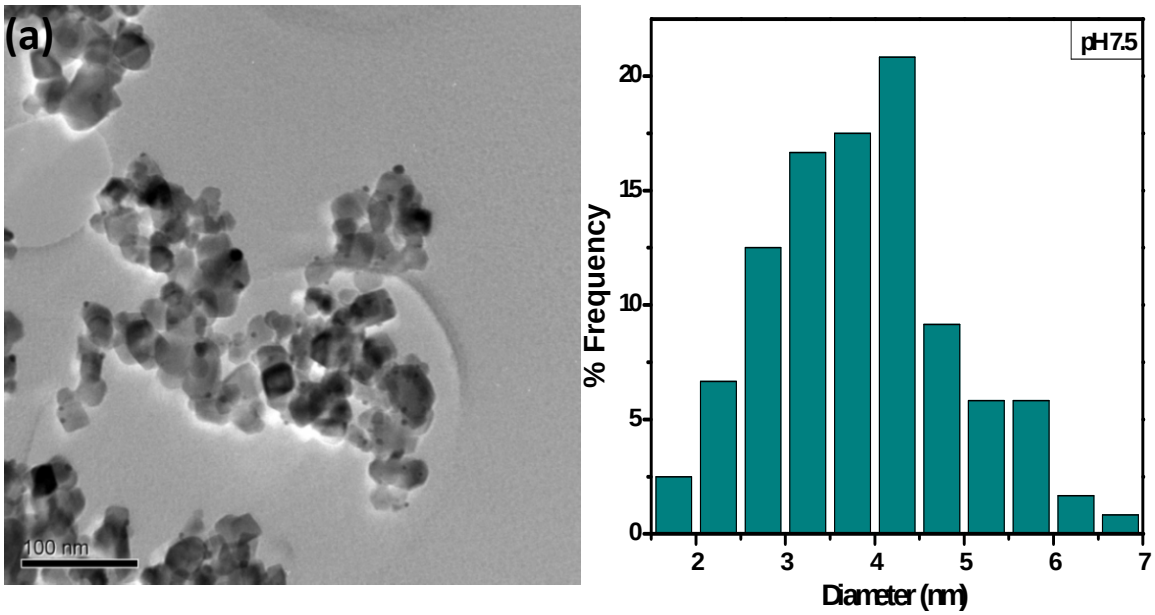

Figure 3.4a: TEM image and average particle size distribution of Au/TiO_2 catalyst of pH 7.5 and 3% metal loading (theoretical loading). Good dispersion of hemispherical and spherical particles can be seen. The particle size distribution was obtained by counting more than 100 particles and determining their size.

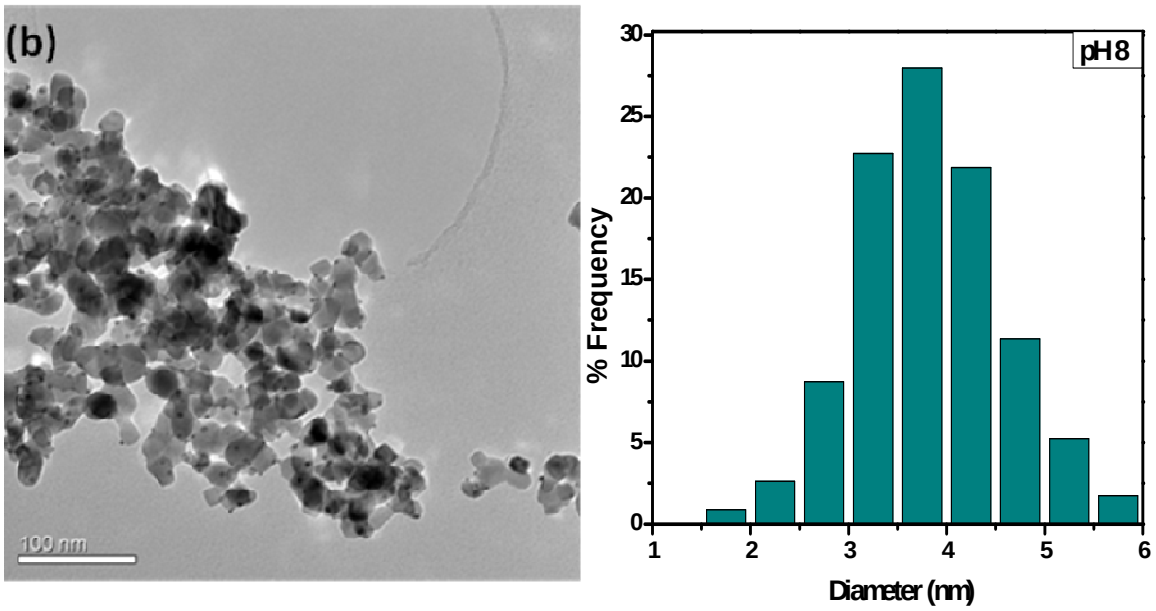

Figure 3.4b: TEM image and average particle size distribution of Au/TiO_2 catalyst of pH 8 and 3% metal loading (theoretical loading). Good dispersion of hemispherical and spherical particles can be seen. The particle size distribution was obtained by counting more than 100 particles and determining their size.

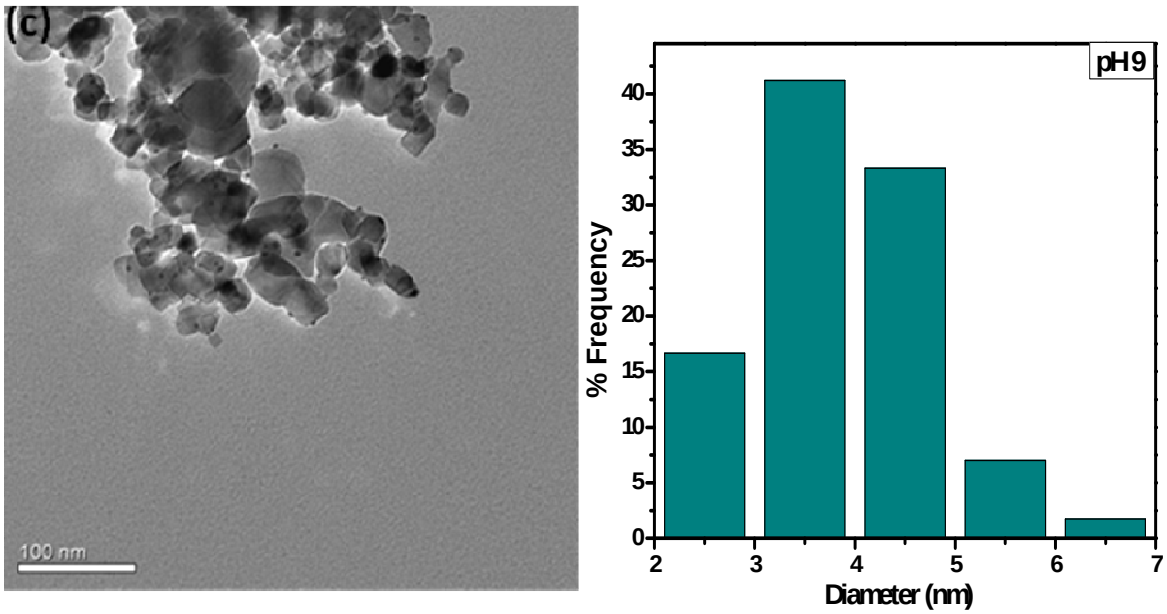

Figure 3.4c: TEM image and average particle size distribution of Au/TiO_2 catalyst of pH 9 and 3% metal loading. Good dispersion of hemispherical and spherical particles can be seen. The particle size distribution was obtained by counting more than 100 particles and determining their size.

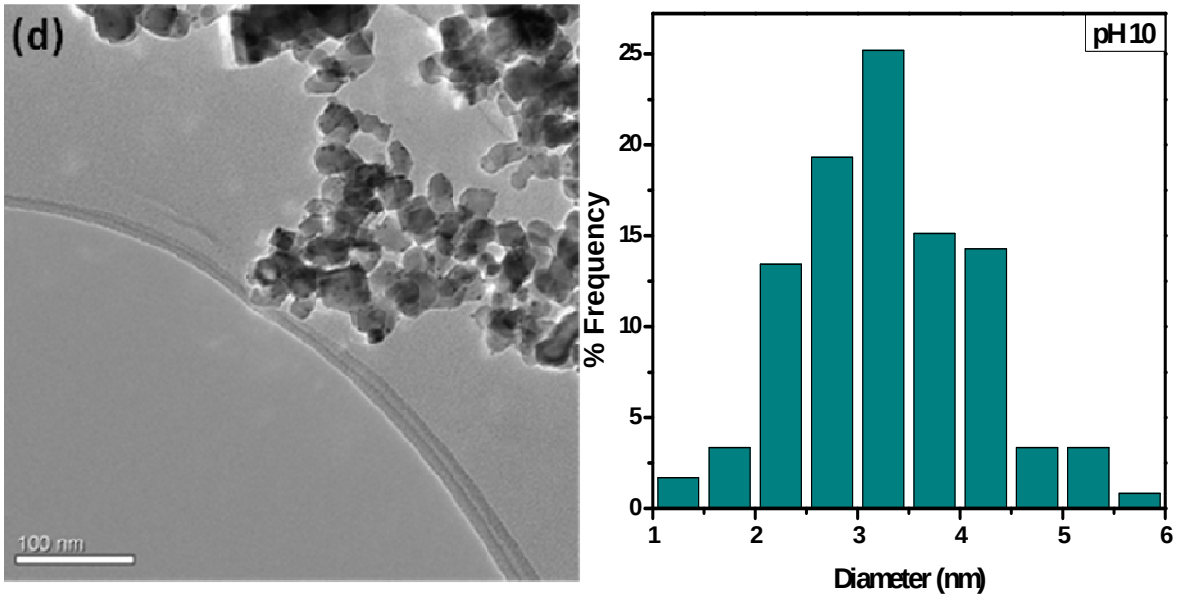

Figure 3.4d: TEM image and average particle size distribution of Au/TiO_2 catalyst of pH 10 and 3% metal loading (theoretical). Good dispersion of hemispherical and spherical particles can be seen. The particle size distribution was obtained by counting more than 100 particles and determining their size.

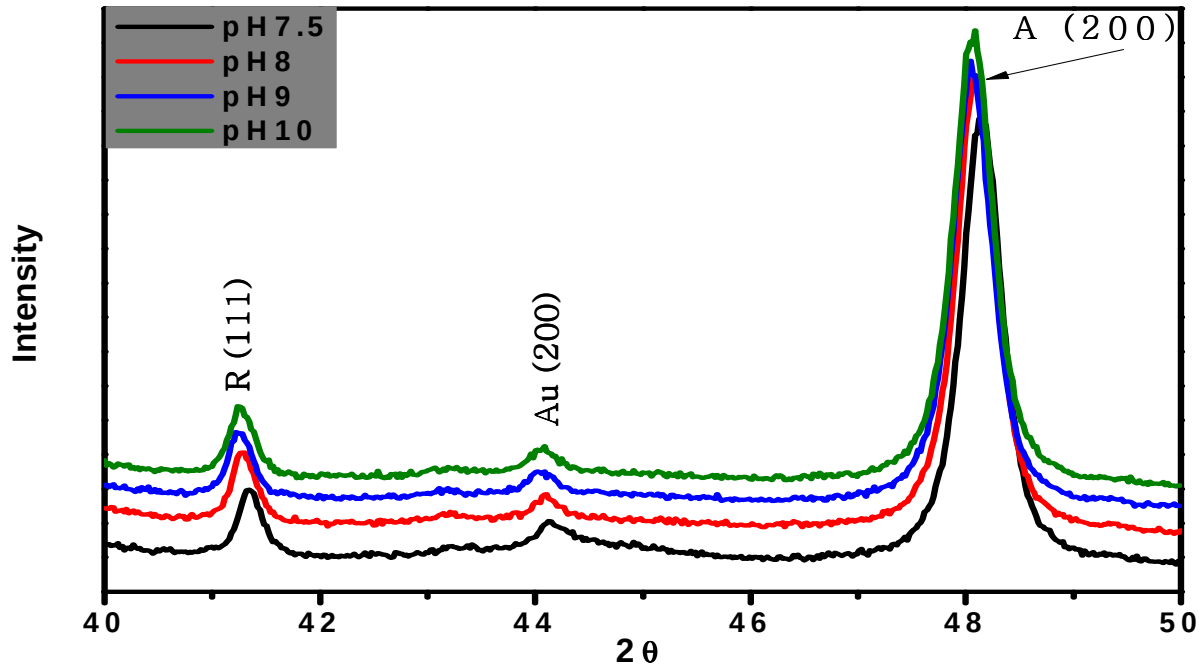

Figure 3.5: XRD patterns of Au/TiO_2 catalysts synthesized at various pH. The letter R and A indicates diffraction peaks for rutile and anatase respectively

3.3.3 The effect of calcination temperature on particle size

Haruta reported that thermal treatment of supported gold catalysts after synthesis is necessary for decomposing oxidic gold species which results in formation of metallic Au species [6]. In some cases it has been reported that thermal treatments converted the support metal oxide from an inactive oxidation state to an active one [6]. For example, for Au/Co oxide and Au/Fe oxide catalysts prepared by coprecipitation method, calcining the freshly prepared catalysts at the appropriate temperature converts the metal oxide to Co_3O_4 and Fe_3O_4 respectively which are the most active forms for CO oxidation [6]. Calcination temperature provides differential characteristics for a catalyst. To study the effect of calcination temperature, the obtained optimum pH 8 and 3% wt loading were the conditions used during synthesis.

For the uncalcined catalysts there were almost no small sized Au particles observed on the TEM image (Fig 3.6a). This is in contrast with the findings of Tanielyan and Augustine who showed that active Au/Fe_2O_3 catalysts could be prepared without heat treatment [20]. The visible black lumpy spots in the TEM images with average size distribution of 14.7 nm (Fig.3.6) suggest poor dispersion of Au particles and the presence of chlorine residual. The visible chloride residual could also indicate that washing catalysts with water was insufficient as reported by Ivanova et al. [21]. Ivanova et.al suggested that additional washing with ammonium solution may replace the chloride ligands of the Au complex thus reducing chloride levels to undetectable limits [21]. Both spherical and hemispherical adsorbed Au particles are visible. In the literature it has been reported that calcination leads to the formation of spherical gold particles being deposited on a metal support [22].

The large visible Au particles on the support could also be an indication that the Au ions were not reduced or there was an inhomogeneous distribution of ammonium across the sample during synthesis. At 200 °C there are small sized Au particles observed indicating full reduction of Au particles which is consistent with the results of Zanella et al who reported full reduction of Au at 200 °C [25]. There is high Au dispersion observed for the catalysts calcined at 200 °C (Fig.3.6b), 300 °C (Fig.3.6c), and 400 °C (Fig.3.6d). The increasing calcination temperature resulted in increased particle size. However, the catalysts calcined at 300 °C showed a decrease in particle size which is in agreement with Daté et al. findings [26]. However, obtained histograms for catalysts calcined at 300 °C does not follow a bell curve which allows normal approximation of random values, whereas a Gaussian curve was observed for catalysts calcined at 200 °C thus becoming an optimum calcination temperature.

It was observed that at 200°C there was a high dispersion of Au nanoparticles adsorbed on the support as indicated by arrows.

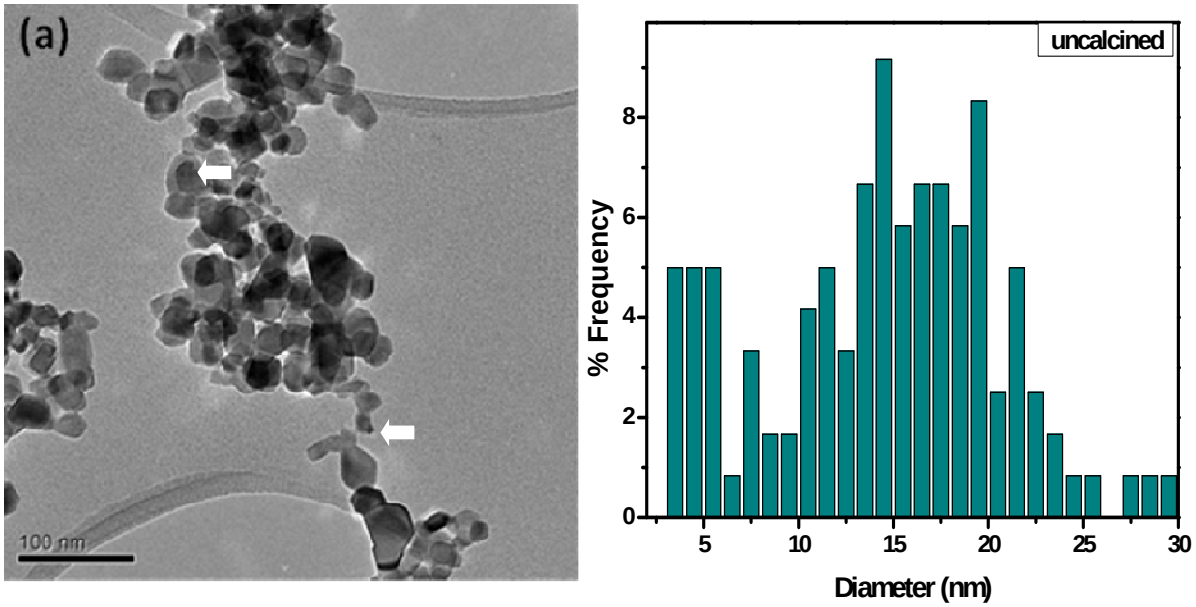

Figure 3.6a: TEM image and average particle size distribution of Au/TiO_2 catalyst of pH 8, 3% metal loading and uncalcined. There are few Au particles that can be seen as indicated by arrows. The particle size distribution was obtained by counting more than 100 particles and determining their size.

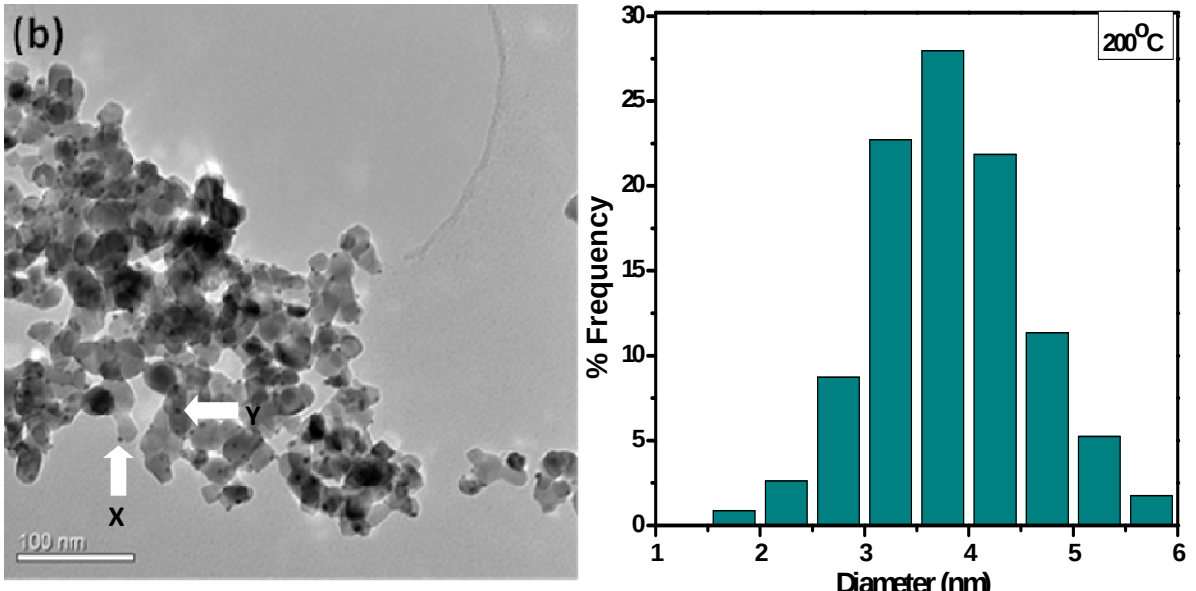

Figure 3.6b: TEM image and average particle size distribution of Au/TiO_2 catalyst of pH 8, 3% metal loading calcined at 200 °C. Good dispersion of hemispherical (***X***) and spherical (***Y***) particles can be seen. The gold loaded is seen as tiny black spots. The particle size distribution was obtained by counting more than 100 particles and determining their size.

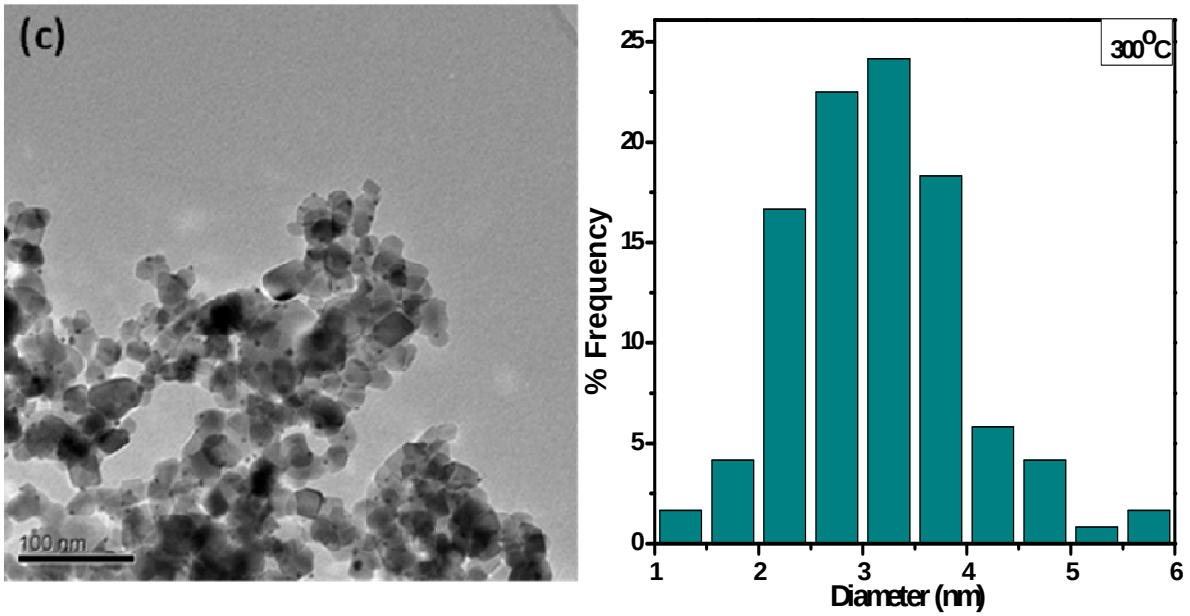

Figure 3.6c: TEM image and average particle size distribution of Au/TiO_2 catalyst of pH 8, 3% metal loading calcined at 300 °C. Good dispersion of hemispherical and spherical particles can be seen. The gold loaded is seen as tiny black spots. The particle size distribution was obtained by counting more than 100 particles and determining their size.

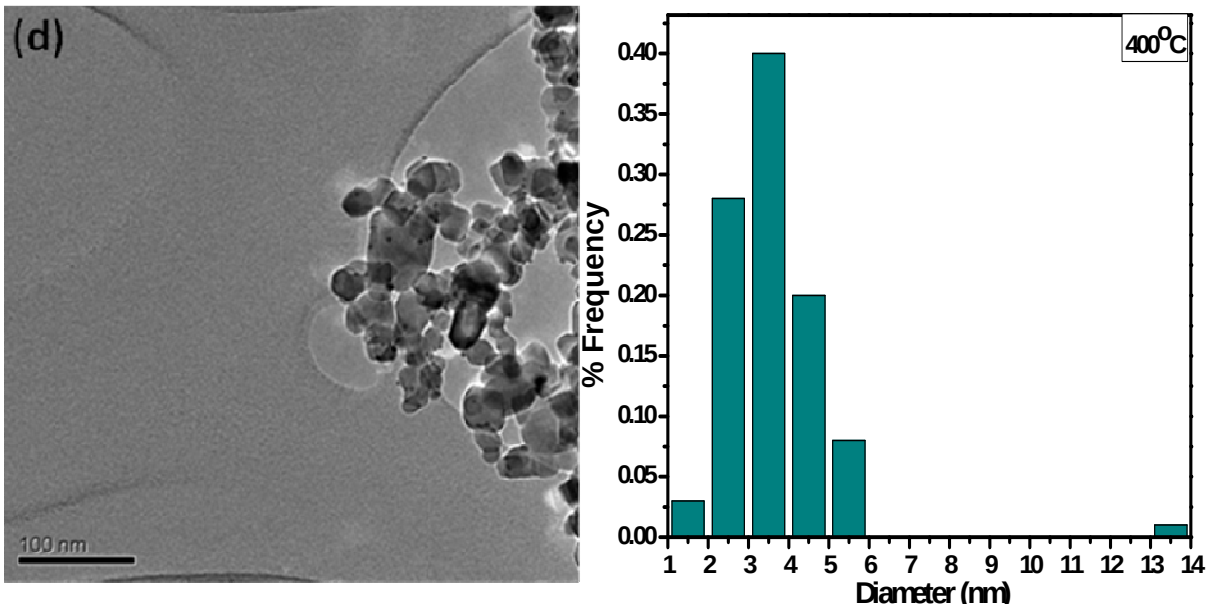

Figure 3.6c: TEM image and average particle size distribution of Au/TiO_2 catalyst of pH 8, 3% metal loading calcined at 400 °C. Good dispersion of hemispherical and spherical particles can be seen. The gold loaded is seen as tiny black spots. The particle size distribution was obtained by counting more than 100 particles and determining their size.

BET studies (Table 3.3) showed a decrease in surface area as the calcination temperature increased. For catalysts calcined at 300 and 400 °C no significant decrease in surface area was observed compared to the catalyst calcined at 200 °C. This suggests that there large Au

particles loaded on the support. It was also observed that there is an increase in pore volume of the catalyst calcined at 400 °C that can merely be attributed to poor dispersion of particles. The XRD diffraction patterns (Fig 3.7) confirm the particle size increases with increasing calcination temperature. However, the calculated crystal size in Table 3.3 is in agreement with TEM results. The obtained crystallite size could be attributed to damage that might have been caused by x-ray during measurements.

Table 3.3: Properties of prepared catalysts with 3% metal loading experimentally determined surface areas (S_{BET}) and average particle size after DP at pH 8 and various calcination temperatures.

Actual Loading	Calcination Temperature °C	S_{BET} ($m^2 g^{-1}$)	Pore Volume ($cm^3.g^{-1}$)	Particle size[a] (nm)	Particle size[b] (nm)
2.45 Au/TiO_2	Uncalcined	37.36(12) [c]	0.3497	14.7	10.6
2.89 Au/TiO_2	200	44.07(3.1) [c]	0.3351	3.7	5.3
2.53 Au/TiO_2	300	35.87(16) [c]	0.3319	3.5	4.3
2.93 Au/TiO_2	400	35.81(16) [c]	0.3636	4.7	7.1

[a] TEM [b] XRD [c] % Error

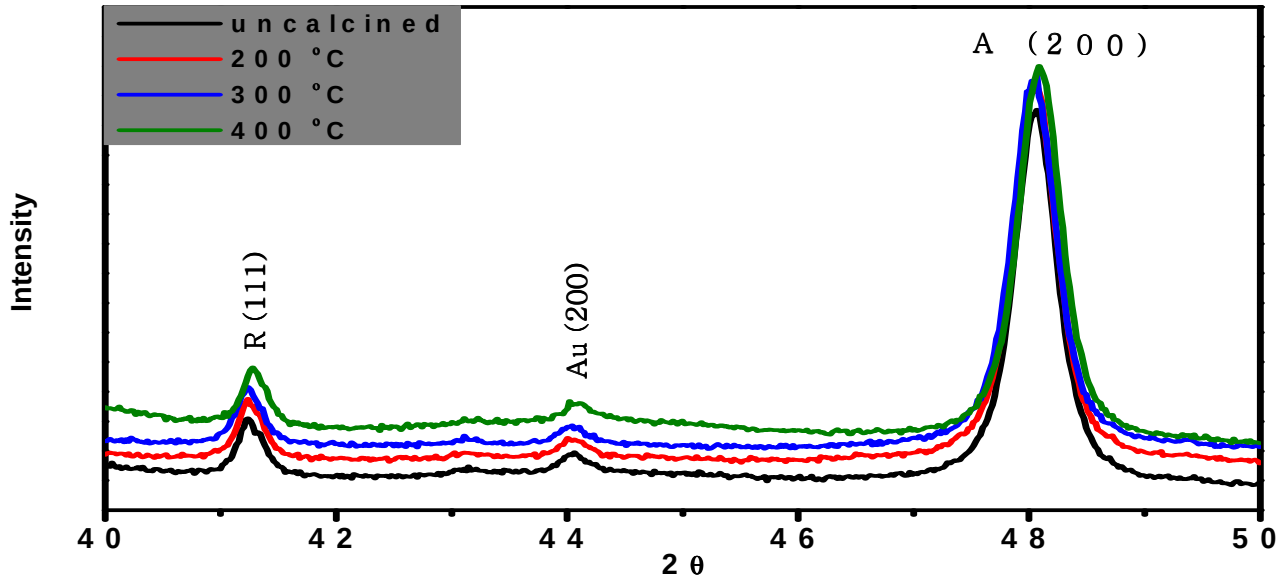

Figure 3.7: XRD patterns of Au/TiO_2 catalysts with 3% Au loading synthesized at pH 8 calcined at various temperatures with the letter R and A indicating diffraction peaks for rutile and anatase respectively.

3.3.4 The effect of aging on particle size

The length of time that the support and the gold precursor are allowed to mix is also reported to affect catalytic performance, presumably because a finite time may be required in order to achieve speciation of the gold [25]. As such preparation time and aging after preparation are equally important if highly monodispersed Au catalysts are to be synthesized. The effect of aging was studied using the catalysts synthesized according to the obtained optimum parameters. TEM images shows that as aging time increased particle size decreased. A decrease in particle size could be attributed to highly dispersed Au particles and less adsorption of chlorine contaminants on the support. These results are consistent with the findings of Lin and Wang who showed that the gold loading increased with the increased aging [28]. They ascribed the increase in loading to more gold being deposited on the exterior surface of the zeolites [26].

The average particle size obtained from TEM (Fig.3.8b and 3.8c) results show that for catalysts aged for 72 h and 24 h has Au particles of size 3.7 nm. However, for catalysts aged for 24 h the histograms shows not normal distribution of particle size which makes these results statistically inconclusive. XRD results, shown in Fig 3.9, confirm that as maturation time increases, particle size decreases. However, the measured crystallite sizes from XRD are inconsistent with TEM results as the large values were obtained. This could be due to XRD measurements taken from a small scan range of 40 to 50 2θ. It is observed that the Au (200) peak is becoming less broad as aging is increased.

Tran et al concluded that maturation time would mainly impact on the chlorine elimination and hence too short maturation time would not allow a sufficiently high pH [27]. Observed surface area (Table 3.4) increases as duration of aging increases indicating adsorption of small Au particles on the support. This result is in agreement with the TEM and XRD results. XRD results shows a decreasing trend in particle size as the aging period increases. However, it is observed that the pore volume decreases with increasing maturation time suggesting that the pores are blocked by Au particles. However, these results shows that increased maturation time facilitates adsorption of small particles on to the support thus aging for 72 h showed Au particles with the smallest particle size of 3.7 nm.

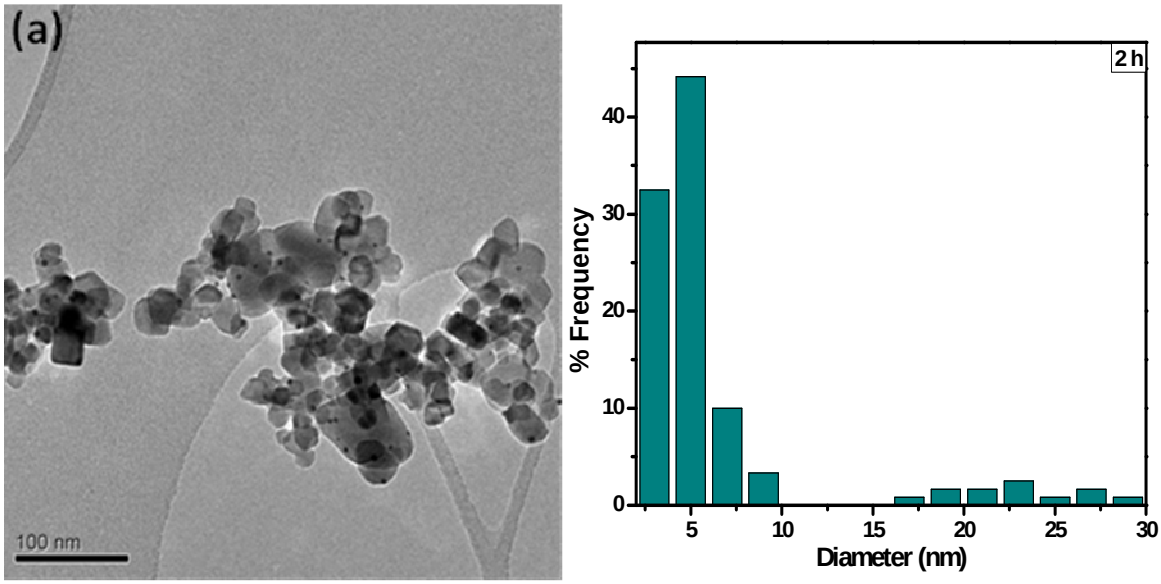

Figure 3.8a: TEM micrograph and average particles size distribution of Au/TiO_2 catalyst of pH 8 with 3 % metal loading, aged for 2 h and calcined at 200 °C. The black tiny particles seen are the Au loaded on the support. The particle size distribution was obtained by counting more than 100 particles and determining their size.

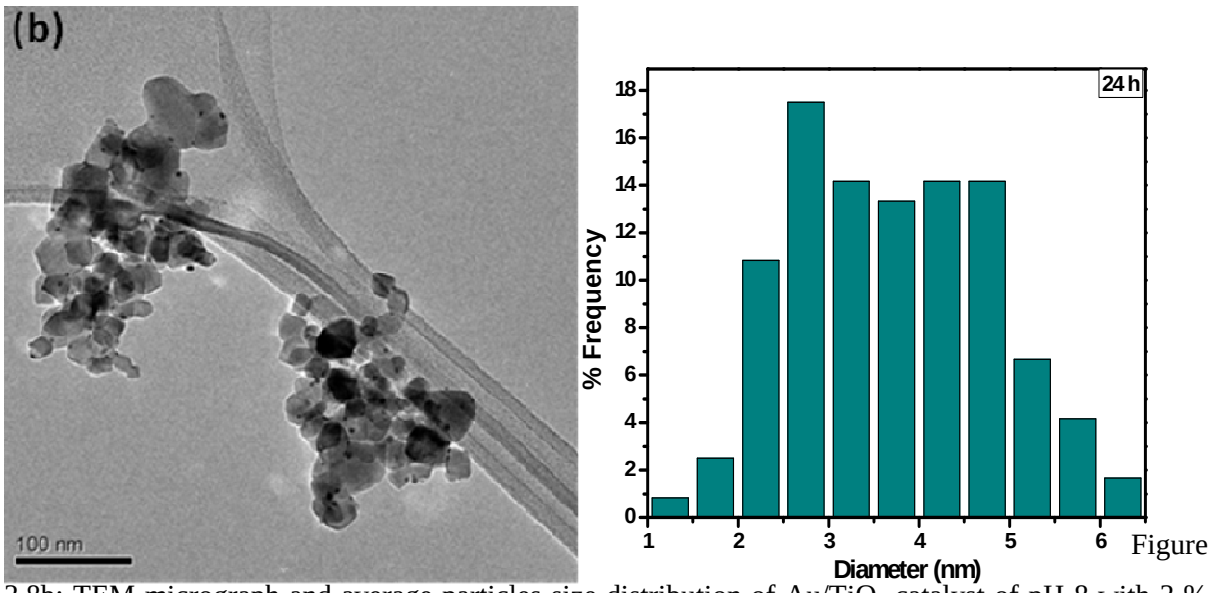

Figure 3.8b: TEM micrograph and average particles size distribution of Au/TiO_2 catalyst of pH 8 with 3 % metal loading, aged for 24 h and calcined at 200 °C. The black tiny particles seen are the Au loaded on the support. The particle size distribution was obtained by counting more than 100 particles and determining their size.

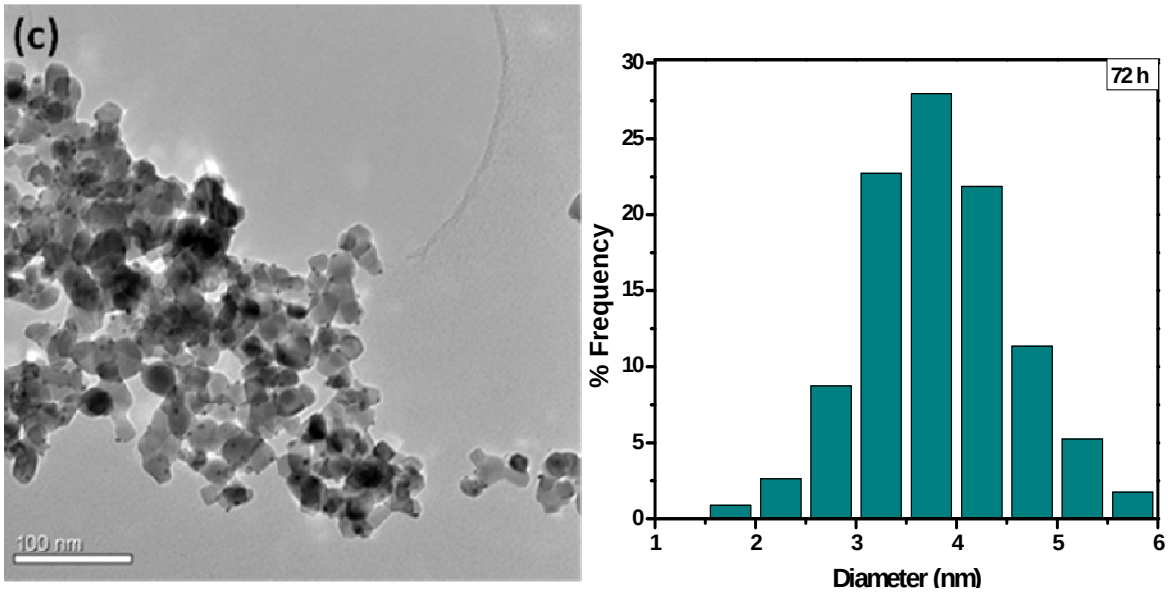

Figure 3.8c: TEM micrograph and average particles size distribution of Au/TiO_2 catalyst of pH 8 with 3 % metal loading, aged for 72 h and calcined at 200 °C. The black tiny particles seen are the Au loaded on the support. The particle size distribution was obtained by counting more than 100 particles and determining their size.

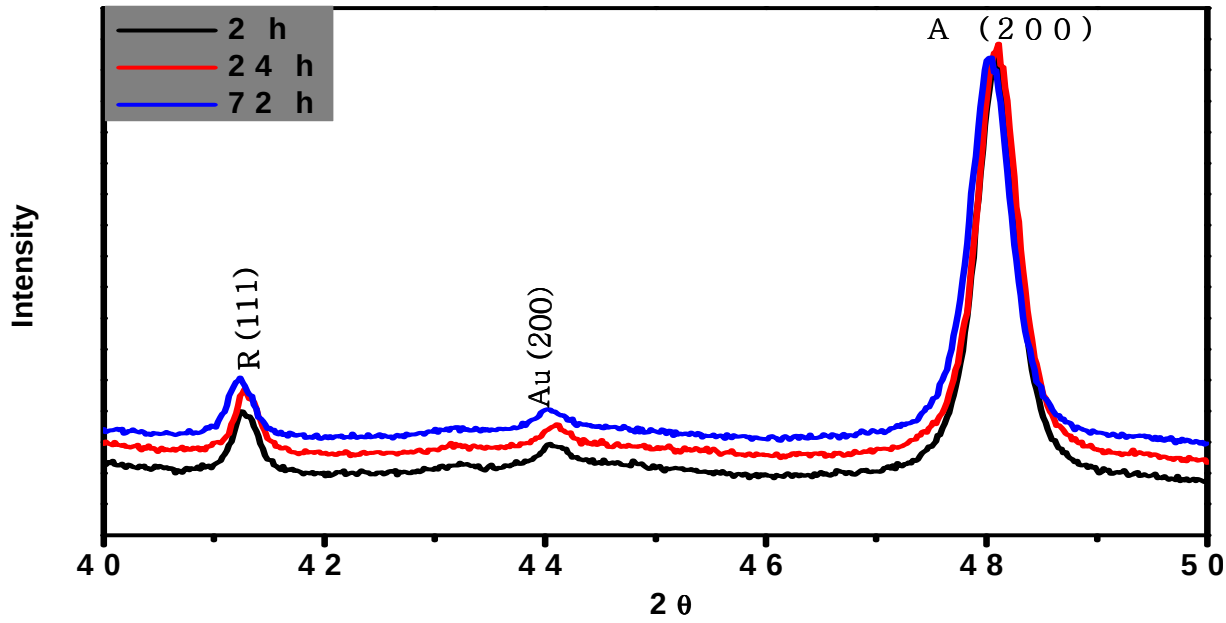

Figure 3.9: XRD patterns of Au/TiO_2 catalysts with 3% Au loading, synthesized at pH 8 calcined at 200 °C aged for various hours.

Table 3.4: Properties of prepared catalysts with 3 % (theoretical loading), of pH calcined at 200 °C while aging period was varied. Surface area (S_{BET}) and average particle size were determined experimentally.

Actual Loading	Aging	S_{BET} ($m^2 g^{-1}$)	Pore Volume ($cm^3.g^{-1}$)	Particle size[a] (nm)	Particle size[b] (nm)
2.63 Au/TiO_2	2 h	37.36(12) [c]	0.3497	5	8.9
2.89 Au/TiO_2	24 h	40.38(5.4) [c]	0.3400	2.7	5.6
2.94 Au/TiO_2	72 h	44.07(3.1) [c]	0.3351	3.7	5.3

[a] TEM [b] XRD [c] % Error

3.3.5 The effect of support on particle size

It has also been reported that one of the critical central issues in gold catalysts used for CO oxidation is the nature of the support material as well as its physical state [29-31]. The typical metal oxide support used for gold catalysts have been identified as either reducible or non-reducible. It has been reported that non-reducible supports such as SiO_2 and Al_2O_3 generally exhibit low activity and that improved activities with them could only be achieved with very small gold particles. In an attempt to study the effect of the support, SiO_2 was used as support material for Au catalyst, while keeping all other optimum conditions from TiO_2 the same except pH. The catalysts were synthesized via the DP method. The Au was precipitated at pH 7 and pH 9. The Au metal loading of the synthesized catalysts was 3%.

TEM results (Fig 3.10a) show amorphous SiO_2 and Au particles as black tiny spots indicated by blue and red arrow respectively. At pH 7 it is observed that there are big lumpy particles indicated by white arrows. The observed large Au particles could be due to poor control of pH during synthesis. Synthesis of Au/SiO_2 at pH 7 was repeated and there was significant decrease in pH observed. Wolf and Schüth reported that SiO_2 is an unsuitable support material for catalysts prepared by a deposition-precipitation method due to its isoeletric point which is below 2 [31]. Therefore SiO_2 will not favour adsorption of $[Au(OH)_nCl_{4-n}^-]$ species onto the support. Literature reported that to overcome the obstacle of adsorbing $Au(OH)_4$ species onto the negatively charged SiO_2 surface under basic conditions, introduction of a high isoelectric point metal oxide onto the SiO_2 surface is important [32-33]. However, the study shows that Au particles that adsorbed onto the SiO_2 tend to be spherical.

It was observed that the obtained average particle size for both pH 7 and 9 was 4.5 nm. Overbury et al. showed that by developing mesoporous supports with mean pore diameters enable strong adsorption of small sized Au particles onto the silica support [32]. It was further reported that functionalizing the silica mesopore walls stabilize Au particles thus prevent particle sintering [34]. Literature indicated that variation of the Au particle size also results in variation in Au-support contact area and possible electronic modulation by the support. Post-modification and pre-modification of the support are indeed vital for obtaining improved electronic structure. Other authors attributed poor Au dispersion to particle size of the support which has the ability to create more contact between the metal [35]. The morphology of the support plays a vital role. Yan and co-workers studied gold nanoparticles supported on γ-Al_2O_3 nanofibers and found it was highly active for CO oxidation as compared to the gold supported on commercial γ-Al_2O_3 [36].

From the XRD pattern (Fig 3.11b) both Au (111) and Au (200) reflections are observed at 2θ= 38 ° and 44° respectively. It was also observed that intensity of Si (111) peak increased suggesting high content of silica. Only the Au (200) peak at 2θ = 44.4° was used to obtain the crystallite size. The obtained results show crystallite size of 4.5 nm which corresponds to TEM results.

It was observed from HRTEM image (Fig 3.11a) for pH 7 the particles coagulated forming one big particle. This indicated that sintering occurred and there poor particle dispersion as well as weak support interactions. It was thought that particle growth could be promoted by chlorine contaminants that are known to facilitate adsorption of large particles on to the support. It can be said that the lumpy particle suggests poor consumption of hydroxyl ions. It is also known that the Au/support interface energy is an important parameter that determines the final shape and size of the Au particles [36-37]. HRTEM showed spherical Au particles anchored weakly onto the support. The absence of hemispherical Au particles on the support indicated that the support helps to determine the shape of the Au particles, in agreement with literature [38-39]. Formation of lumpy particles can also be attributed to morphology of the support modification. These findings confirm that the choice of support plays a vital role in determining Au particle size and shape. The TiO_2 support gave small, well bound particles compared to SiO_2. These results are in agreement with the literature.

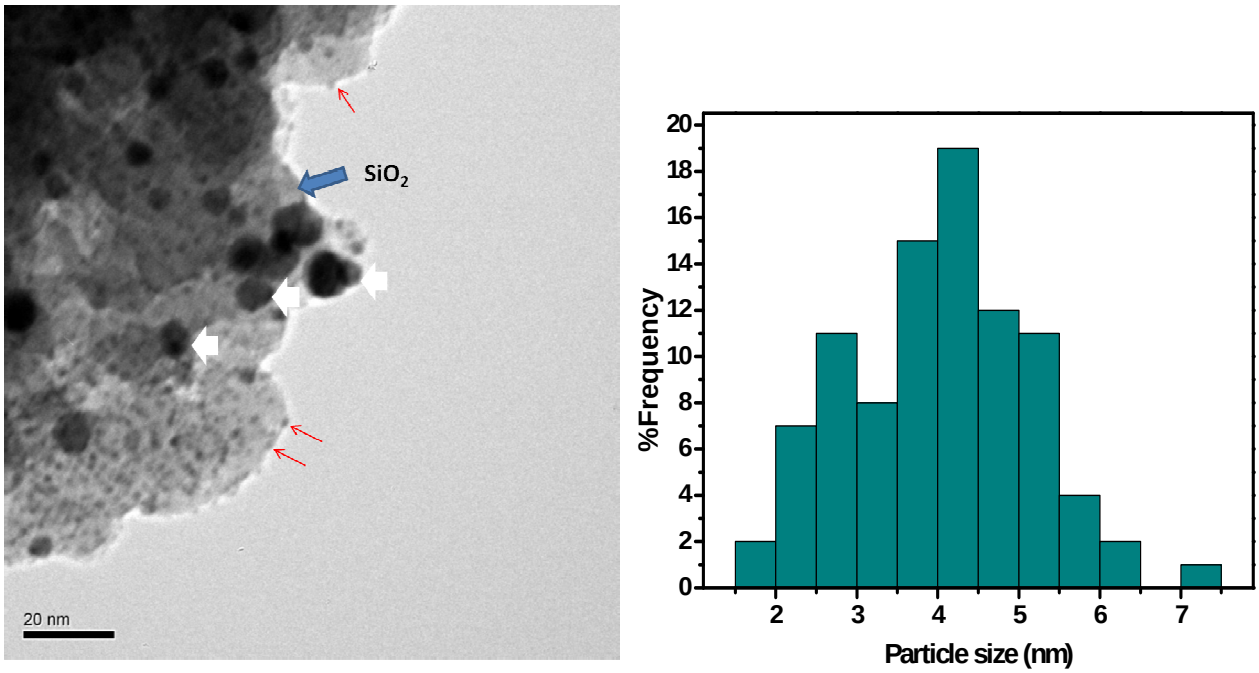

Figure 3.10a: TEM image and average particles size distribution of Au/SiO_2 catalyst with 3% metal loading, synthesized at pH 7 calcined at 200 °C and aged for 72 hours. SiO_2 support is indicated by a blue arrow. The tiny black spots indicated by red arrows shows gold loaded on the support. The black lumpy particles are suspected to be the chlorine contaminants.

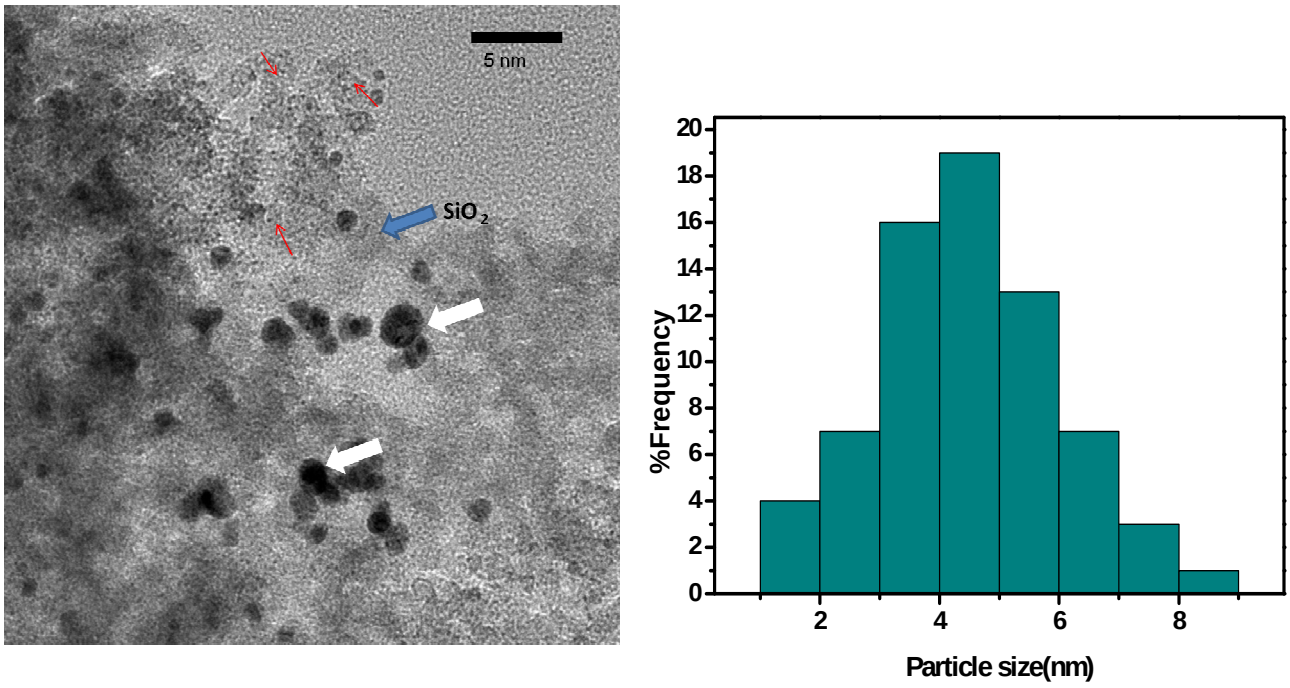

Figure 3.10b: TEM image and average particles size distribution of Au/SiO_2 catalyst with 3% metal loading, synthesized at pH 9 calcined at 200 °C and aged for 72 hours. SiO_2 support is indicated by a blue arrow. The tiny black spots indicated by red arrows shows gold loaded on the support. The black lumpy particles are suspected to be the chlorine contaminants.

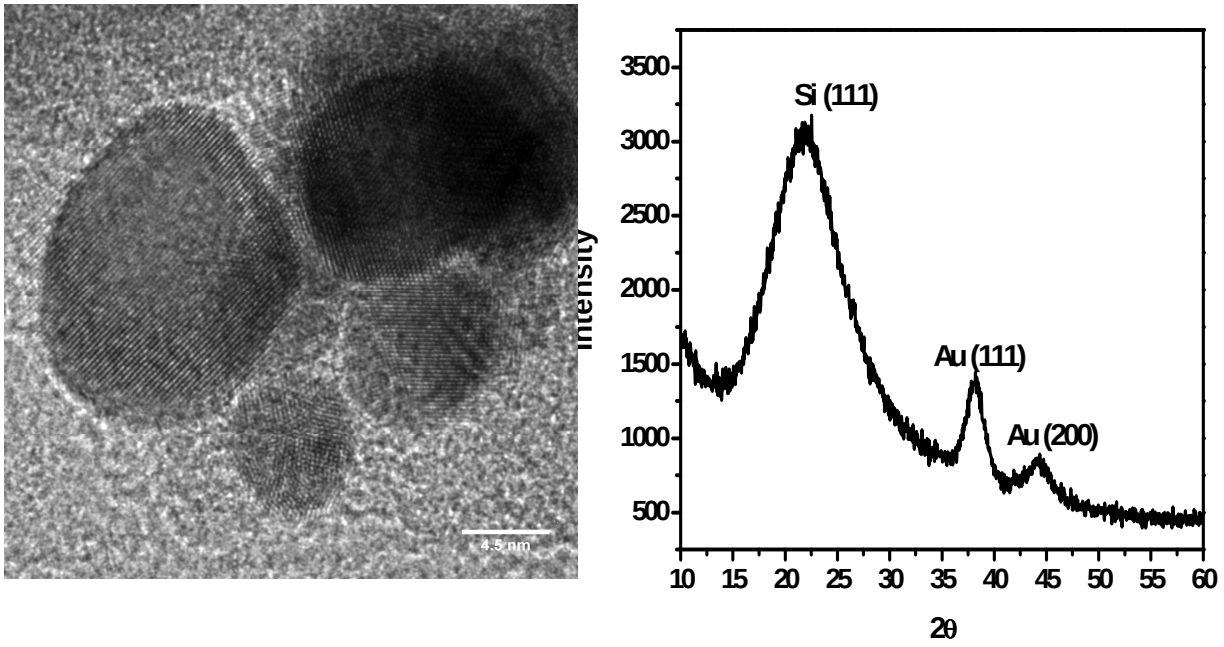

Figure 3.11a: HRTEM image and XRD pattern of Au/SiO_2 catalyst of pH 7. Different sized gold particles can be seen. Formation of one large particle is seen as two particles combines.

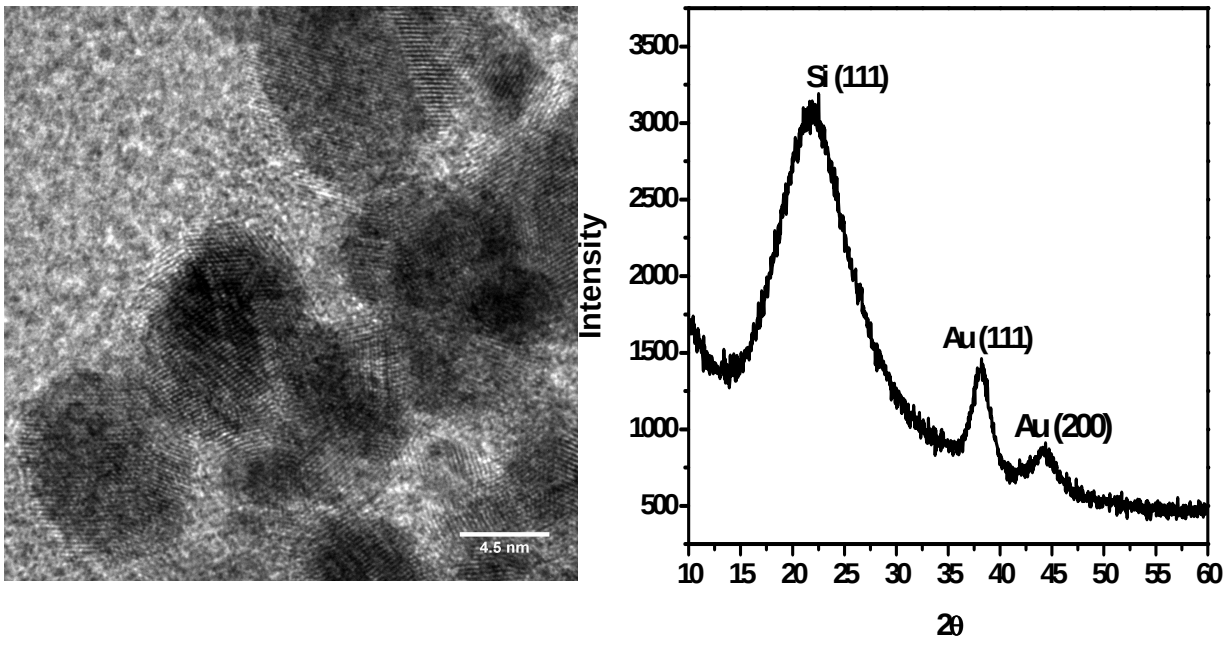

Figure 3.11b: HRTEM image and XRD pattern of Au/SiO_2 catalyst of pH 9. The large particle aggregates can be seen.

BET results (Table 3.4) revealed that SiO_2 has a large surface area compared to P25 degussa. The measured crystal size from XRD and TEM are the same. There is no significant increase in surface area suggesting that the SiO_2 surface was not fully covered by Au particles. Therefore Au particles only occupied just a small portion of the support this is indicated by

change in pore volume. The pore volume of SiO_2 increased with increasing pH suggesting that most Au species were adsorbed on the pores.

Table 3.5: Properties of the Au/SiO_2 prepared catalysts of various pH with surface areas (S_{BET}) and average particle size.

Actual Loading	pH	S_{BET} ($m^2 g^{-1}$)	Pore Volume ($cm^3.g^{-1}$)	Particle size[a] (nm)	Particle size[b] (nm)
SiO_2	-	312.	0.7672	-	-
2.63 Au/SiO_2	7	312.25(0.1)[c]	0.9762	4.7	4.7
2.89 Au/SiO_2	9	312.35(0.1)[c]	1.1970	4.7	4.7

[a] TEM [b] XRD [c] % Error

3.5 Bimetallic Au-Pd/TiO_2 catalysts

Compared with the widely used monometallic Au nanoparticles, bimetallic nanoparticles provide considerably higher tunability of their chemical and structural properties and therefore often show superior catalytic properties [40-45]. Physical and chemical properties of a bimetallic catalyst often vary from their single metal counterparts hence contributing to high activity of bimetallic catalysts. The enhanced activity of bimetallic catalysts is usually attributed to the synergistic effects. In particular Au-Pd systems have been extensively studied before as the two metals are miscible and show a high activity and high resistance to oxygen poisoning [41, 47-49]. The synergistic effect between Au and Pd metals is a well known phenomenon [50]. However, segregation of particles or multiple phases have been reported. The segregation of particles results from preparation method or thermal treatments induced after synthesis. The presence of multiple phases poses a difficult task in identifying particles or species responsible for high activity. A high metal dispersion and good particles size control of the Au/Pd system on the activated carbon synthesized via sol-gel technique has been reported in the literature [51].

In an attempt to overcome the sintering of gold nanoparticles in catalysts a bimetallic catalyst was synthesized via the deposition-precipitation method. Palladium metal (classified as platinum group metal (PGM)) was incorporated to enhance the activity and stability of gold catalyst. Palladium metal is known to have high melting temperature 1552 °C [51]. Hence it was hoped that a combination of gold and palladium could be a viable solution for to prevent sintering. Palladium metal is a more economical choice. Therefore it is anticipated that the use of Pd metal may introduce structural modification of the catalysts and the synergistic

effects introduced will enhance the catalysts activity making the catalyst operational under harsh conditions

In this study bimetallic catalysts were synthesized via DP method without the use of any stabilizers. The solutions of Au and Pd ions were mixed and precipitated onto the support while maintaining pH with NH_4OH solution. The mass ratio of Au:Pd were 90:10, 75:25, 50:50 and 25:75 with a total metal loading of 3%. XRD analysis was performed to determine catalyst composition. From the diffraction pattern (Fig 3.12) it was observed that there were no additional diffraction peaks assignable to any palladium compounds such as PdO, metallic Pd or AuPd despite increase in Pd loading. The absence of any palladium compounds could be due to the low loading of Pd used during deposition. There was no evidence from PXRD of the formation of an AuPd alloy. However, the Au (200) peak at $2\theta=44.4°$ was observed. The observed Au (200) peak may indicate deposition of Pd metal on the specific site suggesting formation of heterostructured bimetallic catalysts. Wang et al. and Li et al. indicated that for heterostructure bimetallic compounds, the characteristic diffraction peaks of two kinds of metals can be observed together; while for intermetallics and alloys, the characteristic peaks of individual metals disappear and new Bragg reflections are observed [52]. In contrast to XRD results, ICP analysis showed both Pd and Au metal loading indicating that both metals are adsorbed on the support. The discrepancy could be explained by considering PXRD is a bulk technique and hence not sensitive to small surface deposition percentages.

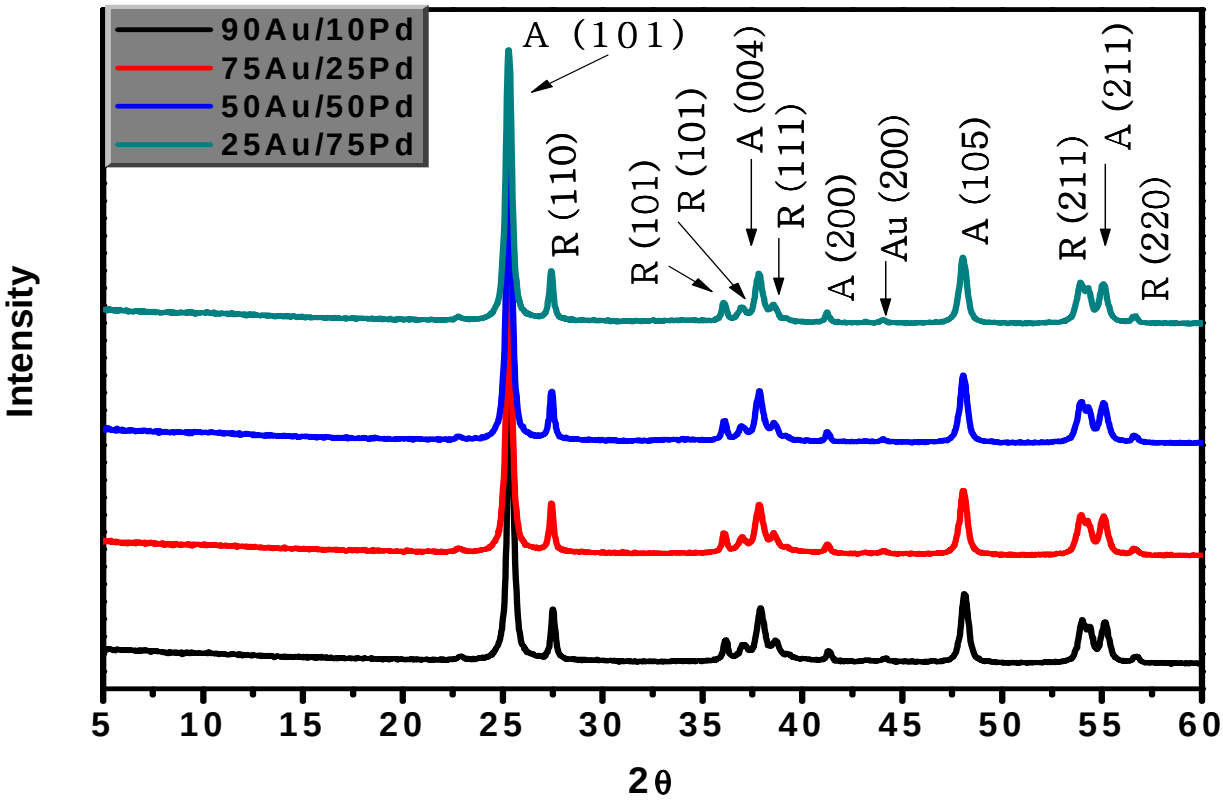

Figure 3.12: XRD analysis of Au-Pd/TiO_2 catalysts with various metal loading. The Letter R and A indicates rutile and anatase respectively.

The bimetallic catalysts were observed by TEM (Fig.3.13). The obtained images showed no distinct Pd and Au particles through colour or morphology. Only tiny black particles were observed. However, it was observed for 22Au71Pd catalysts there were small and medium sized particles attached onto the support. The small sized particles are indicated by letter ***x*** and the medium sized by letter ***y***. It was observed that the particle size decreased with increasing Pd loading. The obtained particle size ranged from 2.5-3 nm. Despite the unknown composition of the visible particles on the surface of the support it was observed that there was high dispersion of small sized particles suggesting good control of pH. BET results (Table 3.6) indicate that there is an increase in surface area as the Pd loading increases except for the 25Au75Pd catalysts with 42.80 m^2 g^{-1} surface area which is equivalent to that of P25 (Degussa). However, there was an increase in pore volume observed compared to that of TiO_2 suggesting that Au particles were blocking the pores. There measured pore volumes are in agreement with the obtained surface area measurements as there is significant increase observed except for that of 25Au75Pd which shows a decrease in pore volume.

Table 3.6: Properties of the Au-Pd/TiO_2 prepared catalysts of various Au and Pd loadings with experimentally determined surface areas (S_{BET}) and average particle size.

Theoretical Loading	**Actual Loading**	**S_{BET} ($m^2 g^{-1}$)**	**Pore Volume ($cm^3.g^{-1}$)**	**Particle size[a] (nm)**
TiO_2 (P25)	-	42.79	0.1526	-
90 Au10Pd	87Au5Pd	40.31(5.8) [b]	0.2893	3.0
75 Au25Pd	69Au20Pd	42.75(0.1) [b]	0.3389	3.0
50 Au50Pd	48Au47Pd	43.75(2.2) [b]	0.3539	2.5
25 Au75Pd	22Au71Pd	42.80 (0.1) [b]	0.3257	2.5

[a] TEM [b] % Error

Further analysis on morphology of the synthesized catalysts was performed by HRTEM. The HRTEM images (Fig. 3.14) show particles of different morphologies deposited on the TiO_2. There are small and medium sized particles observed on the support despite different loadings of both metals. The small particles are indicated by letter ***X*** and the medium sized by letter ***Y***. The different sized particles indicate lack of control of nucleation rate during synthesis. Furthermore the different sized particles also suggest that both metals are separately attached onto the support. The various sized particles could be due to segregation during synthesis. According to literature segregation or multiple phases have been reported in multi-metallic catalytic systems [53]. However, segregation can be influenced by a lot of factors during synthesis. Wang and Li demonstrated that the potential energy gain upon collision of Ag nanoparticles is smaller than that of Pt during synthesis of Pt-Ag by co-reduction method [28]. As such it hinders formation of alloyed particles which ultimately forms heterostructured bimetallic nanoparticles. However, it is difficult to distinguish Au or Pd metals in the obtained HRTEM images since all particles on the support have the same colour and morphology. Hemispherical and spherically attached particles onto the surface of the support were observed.

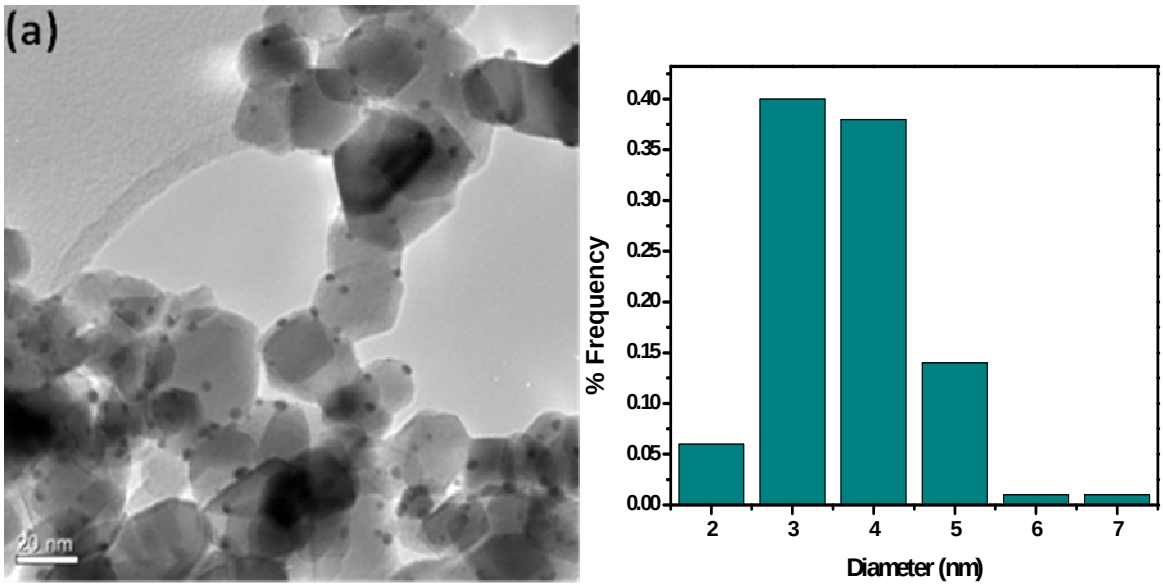

Figure 3.13a: TEM micrograph and particle size distribution of 90Au10Pd catalyst. The Au and Pd metals cannot be distinguished by colour or morphology. Only tiny black particles are visible the support.

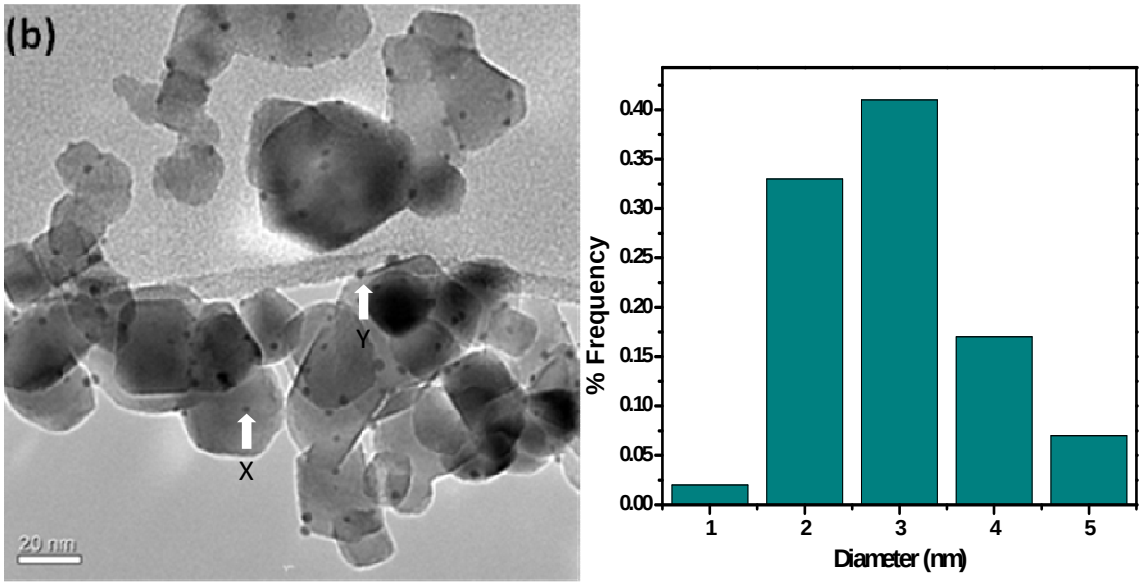

Figure 3.13b: TEM micrograph and particle size distribution of 75Au25Pd catalyst. The Au and Pd metals cannot be distinguished by colour or morphology. A uniform dispersion of tiny black particles can be seen.

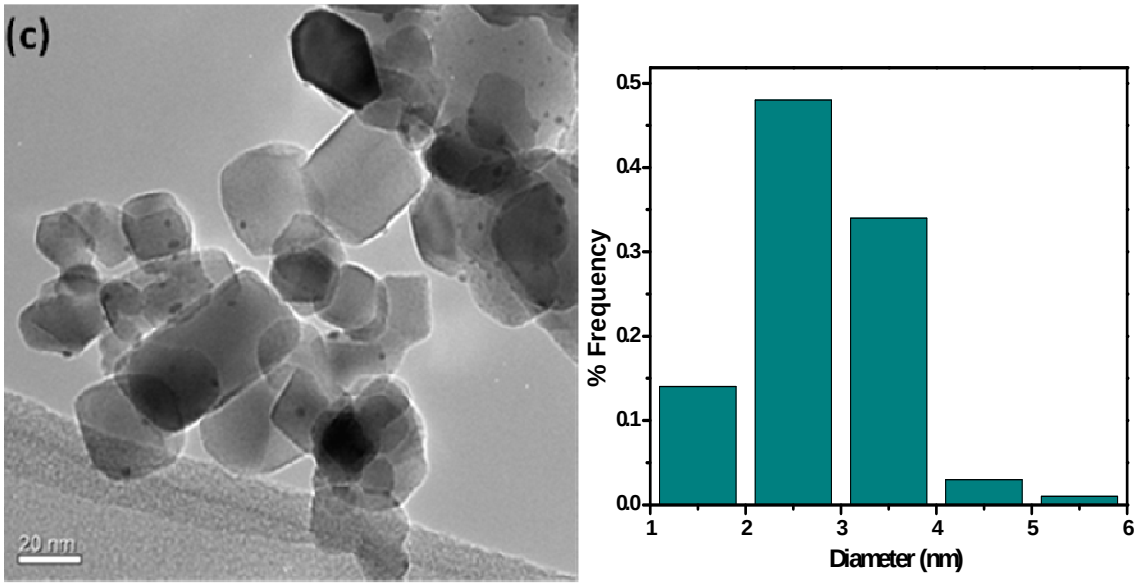

Figure 3.13c: TEM micrograph and particle size distribution of 50Au50Pd catalyst. The Au and Pd metals cannot be distinguished by colour or morphology. Only black tiny particles can be seen on the support.

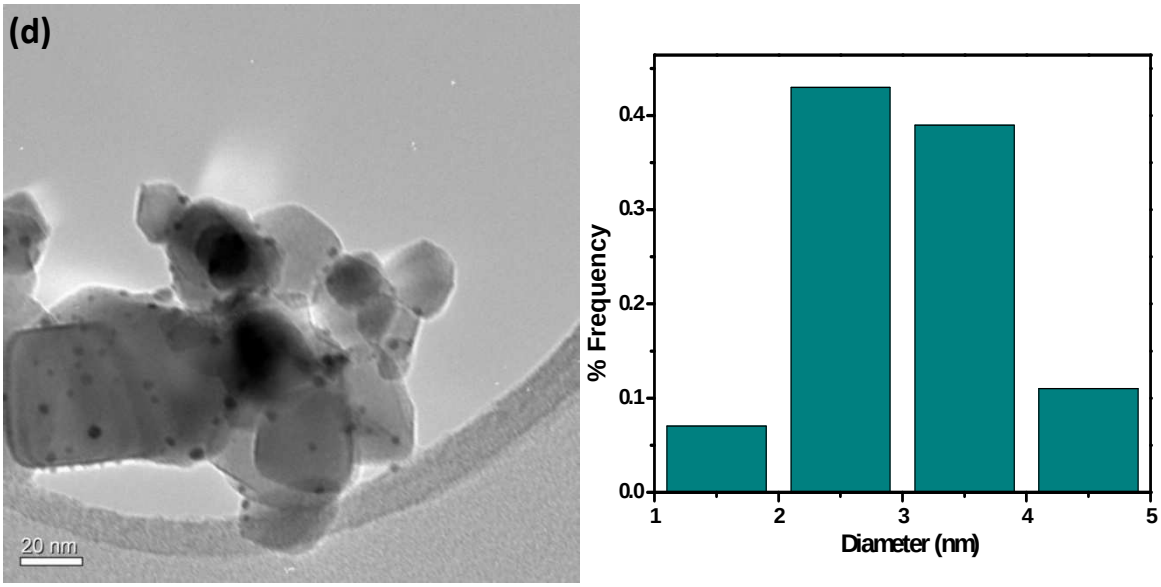

Figure 3.13d: TEM micrograph and particle size distribution of 25Au75Pd catalyst. The Au and Pd metals cannot be distinguished by colour or morphology. Only black tiny particles can be seen on the support.

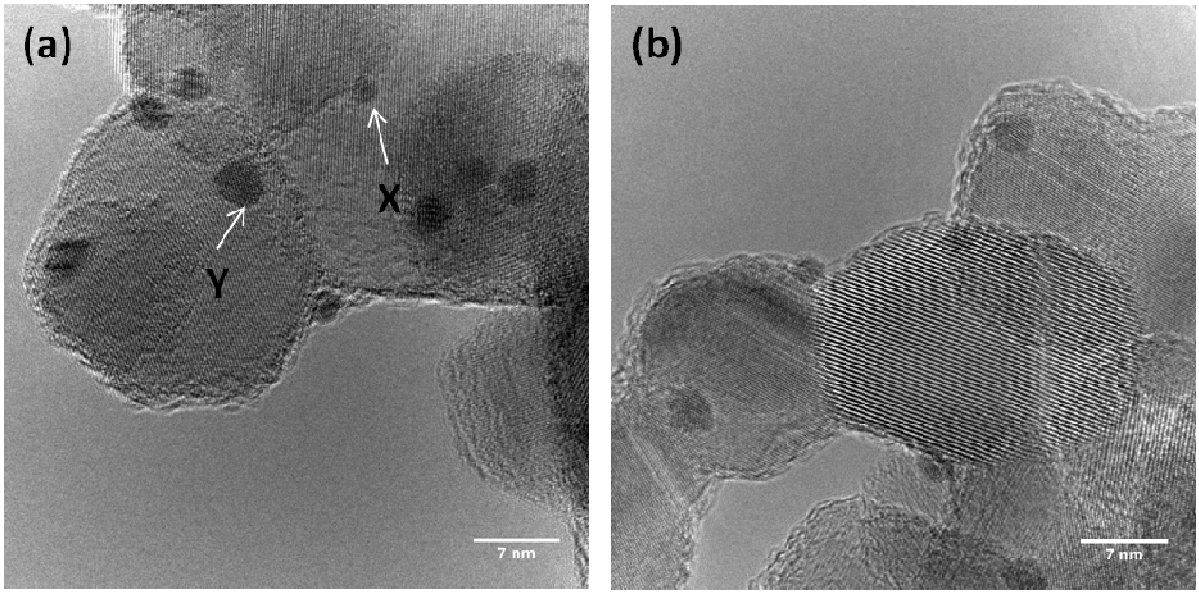

Figure 3.14: HRTEM micrographs of a) 69Au20Pd and b) 48Au47Pd. The X and Y letters indicating small and medium sized particles respectively.

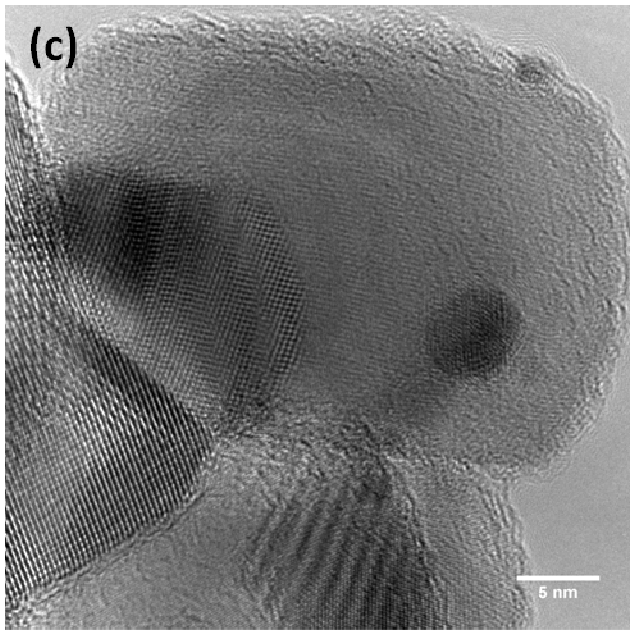

Figure 3.14c: HRTEM micrograph of 22Au71Pd indicating small and medium sized particles.

Elemental analysis by EDS of the prepared bimetallic catalysts is shown below in Figure 3.15. EDS revealed that the synthesized catalysts were composed of Pd and Au metals. The different ratios of metals can also be clearly seen in the spectrum. For an example where there was more Au metal, the Au peak is clearly defined than Pd peak and vice versa. However, for 50Au50Pd catalysts the Au and Pd peaks show equivalent intensity implying the equal amounts of both metals. The EDS results are in good agreement with the obtained

ICP results. The Ti and O peaks results from the support material TiO_2. Copper is detected from the SPI Cu grid used to load the sample during analysis.

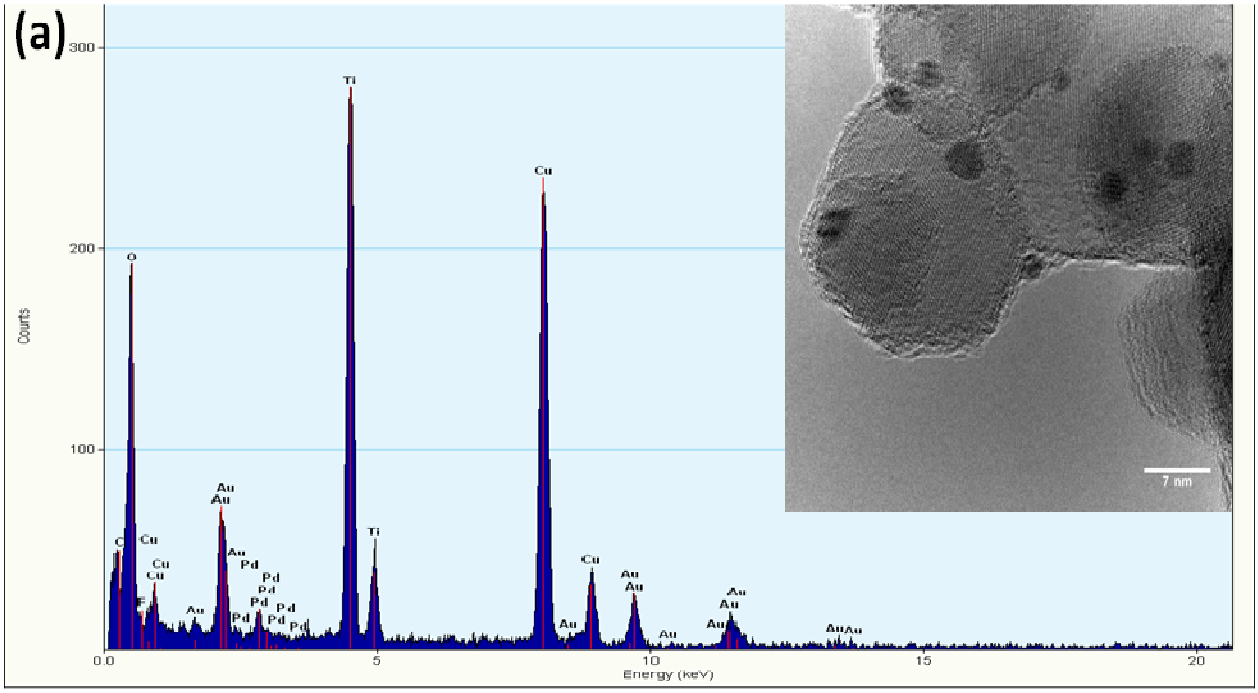

Figure 3.15a: EDS spectrum and HRTEM image of 75Au25Pd

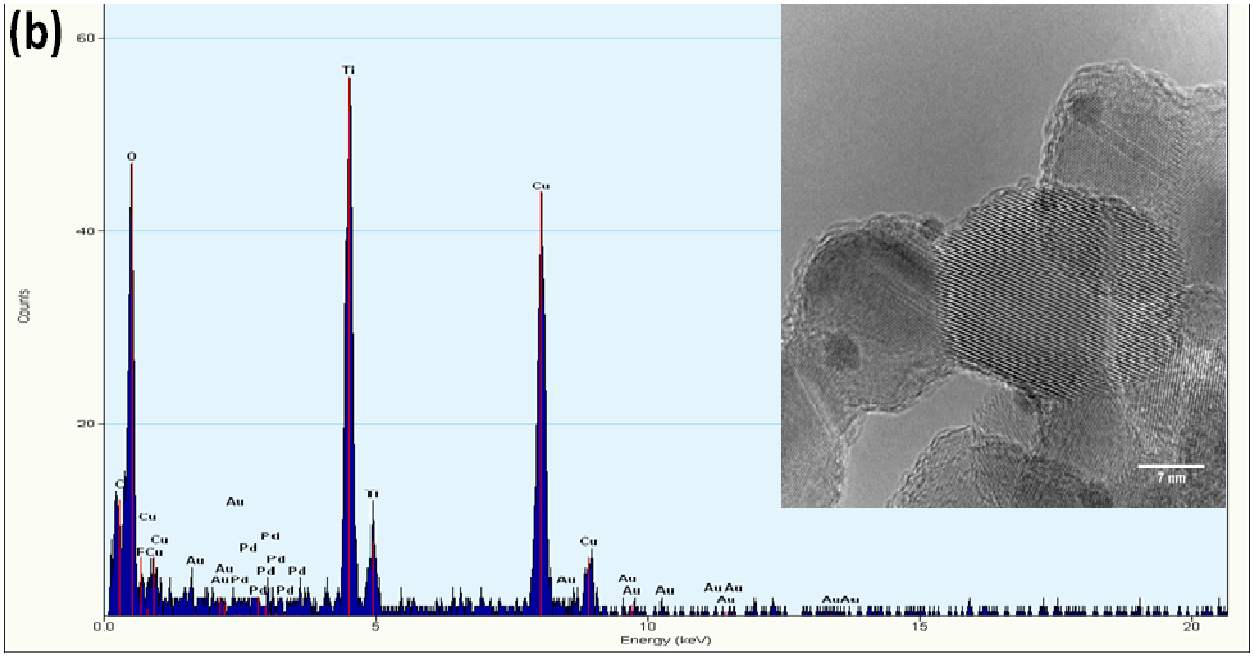

Figure 3.15b: EDS spectrum and HRTEM image of 50Au50Pd

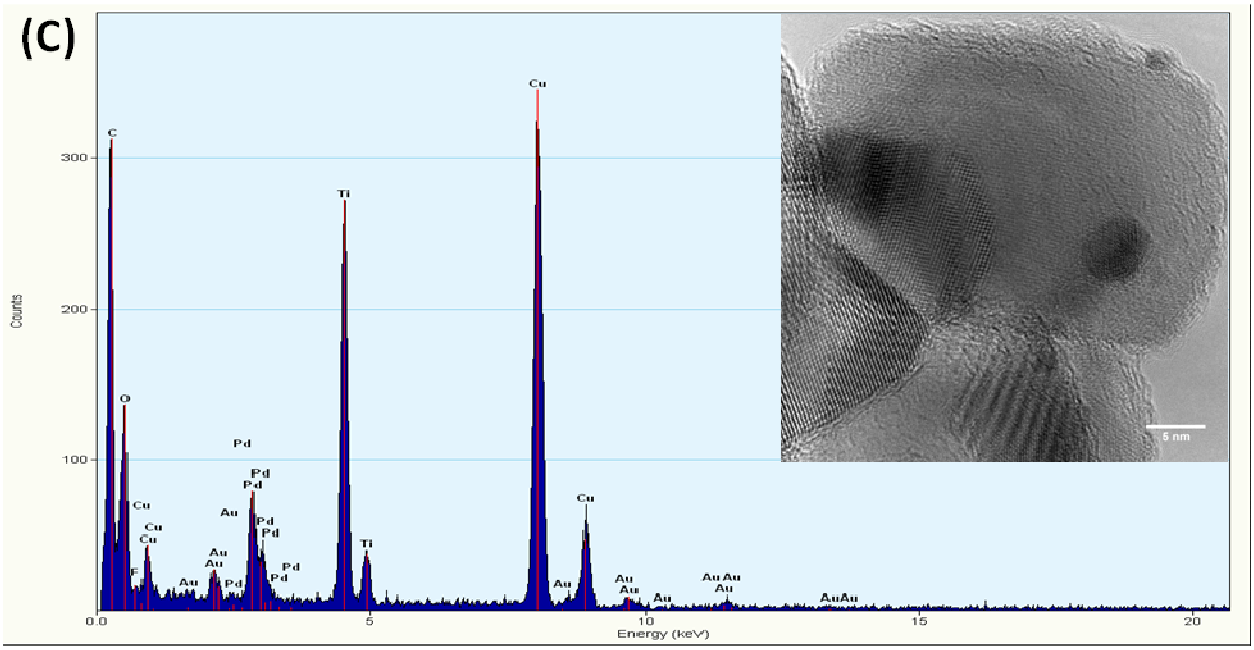

Figure 3.15c: EDS spectrum and HRTEM image of 25Au75Pd

Although the EDS results show deposition of both metals on the support the results are still inconclusive as to whether the bimetallic system formed was heterostructured or an alloy system. Below in Fig 3.16 and Fig 3.17 there is a clear evidence of hemispherical and spherically attached particles onto the support with different morphologies. In Fig 3.16 a top half truncated octahedron particle is observed. The general five-fold symmetry twinned structures is observed in Fig 3.17. The five fold symmetry twinned structures are usually stable in small size [54]. The different morphologies observed show a lack of control over crystal structure.

Lim et al. showed that the resultant nanostructure require manipulation by reducing agents, that is by kinetically controlling the growth rate of crystals [55]. The use of reducing agents is strongly recommended if particular bimetallic particles of specific shape are to be synthesized. The various shaped particle on the support could also be an indication that both metals are separately attached onto the surface of the support. Since it is evident from the EDS analysis that both Pd and Au metals are present, by measuring the lattice distance of the observed particles from the HRTEM images could reveal the type of bimetallic system formed. According to literature the interatomic distance of bulk Au and Pd is 2.9 Å and 2.75Å respectively [56-57]. Similarly the studies conducted by Chen et al showed the Pd-Pd bond distance in Pd/Al_2O_3 was 2.73 Å [42]. In this study the measured interatomic distance of the truncated octahedron shaped particle (Fig.3.16.) is 3.84 Å which is a value close to the

value observed for significant long interatomic Au–Au distances, 3.6–5.0 Å [58-59]. The spherically attached particle in Fig 3.17 exhibits the interatomic distance of 2.68 Å which is very close to that of bulk Pd 2.75Å. These results are in good agreement with the EDS analysis.

The measured interatomic distance suggests the presence of both metals separately attached on the support. Thus, it can be said that heterostructured bimetallic system is formed. It can also be assumed that the medium sized particles attached spherically onto the support are the Au nanoparticles hence XRD was able to show the Au peaks, and the measured interatomic distance is close to that of Au bulk.

However, a decrease in the interatomic distance of the Au metal can be attributed to the interaction with the support which is in agreement with the findings of Rodrigues et al and co-workers. They ascribed the change in bond distance to the presence of impurities [60].

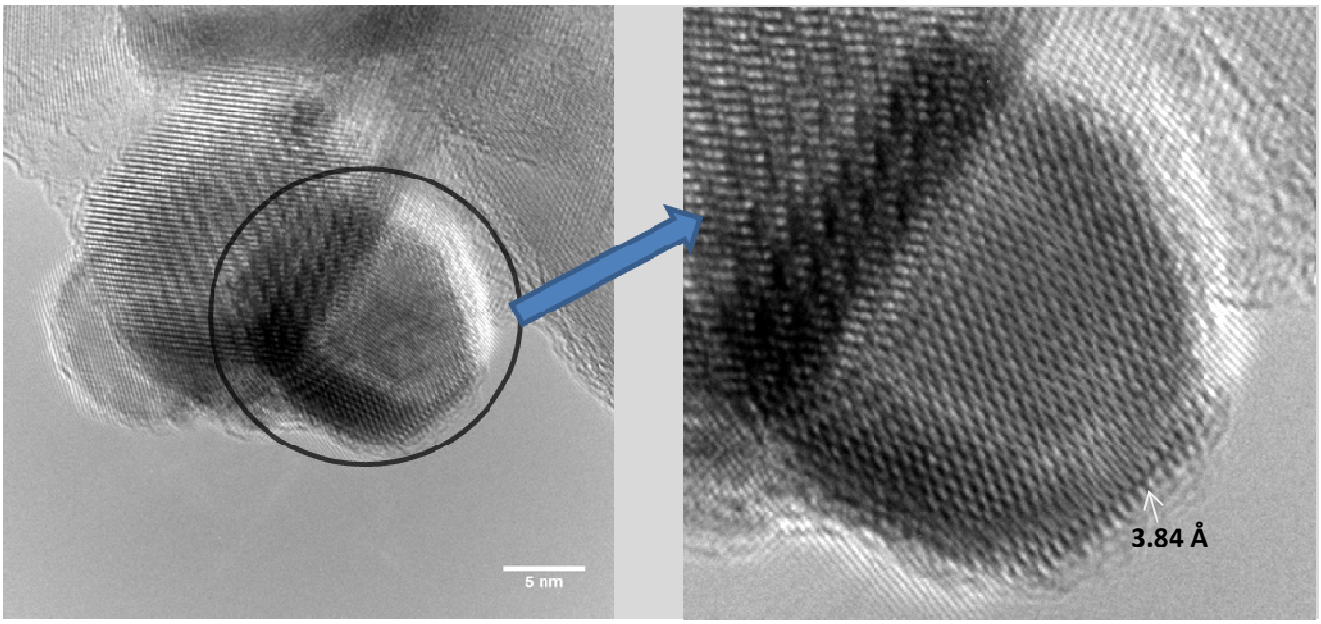

Figure 3.16: HRTEM image showing a top half truncated octahedron particle with the arrow pointing the zoomed area with lattice spacing of 3.84 Å.

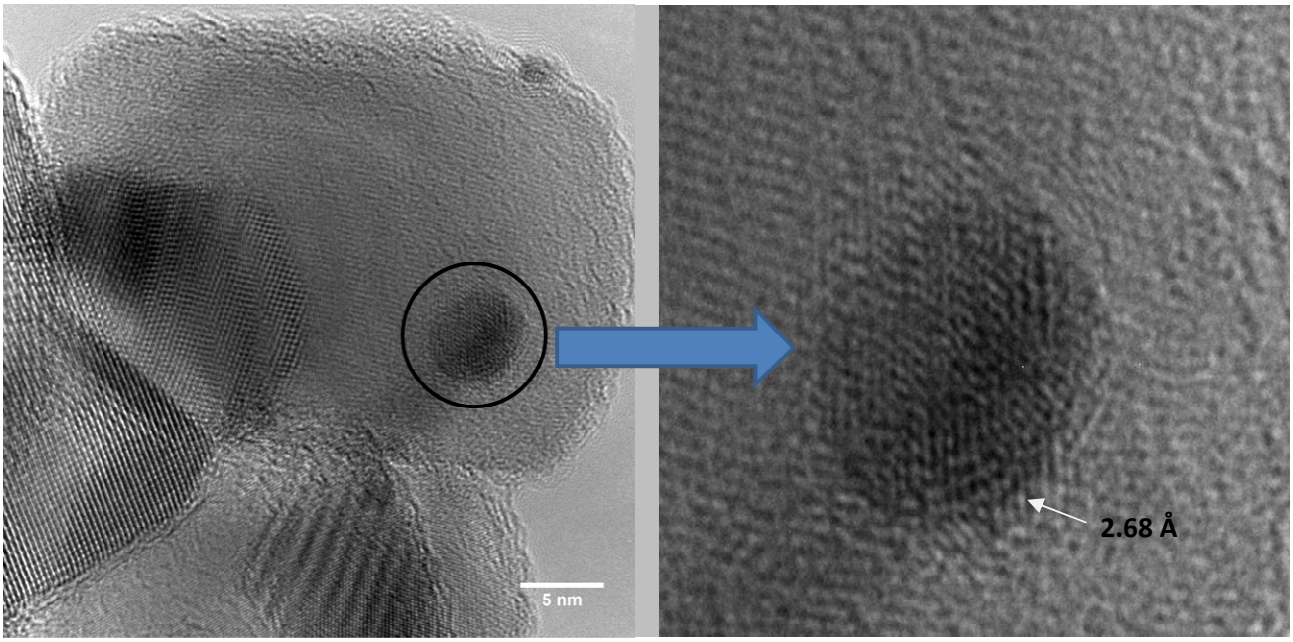

Figure 3.17: HRTEM image showing a different shaped particle spherically attached onto the support. The arrow shows the zoomed area of the particle with 2.68 Å lattice spacing.

The HRTEM also reveals two particles coming together Fig (3.18.) forming one big particle. However, it is not known whether this could be due to coalescence effect or the lumpy particle is composed of both Au and Pd metals. To confirm, the interatomic distance of this particle was measured. The measured interatomic distance obtained was 2.89 Å. The obtained atomic distance is very close to that of Au metal 2.9 Å. This result is in agreement with the XRD analysis. Therefore formation of big particles can be attributed to particle sintering which shows a lack of pH control during synthesis. Thus separate adsorption of both Au and Pd metals is confirmed.

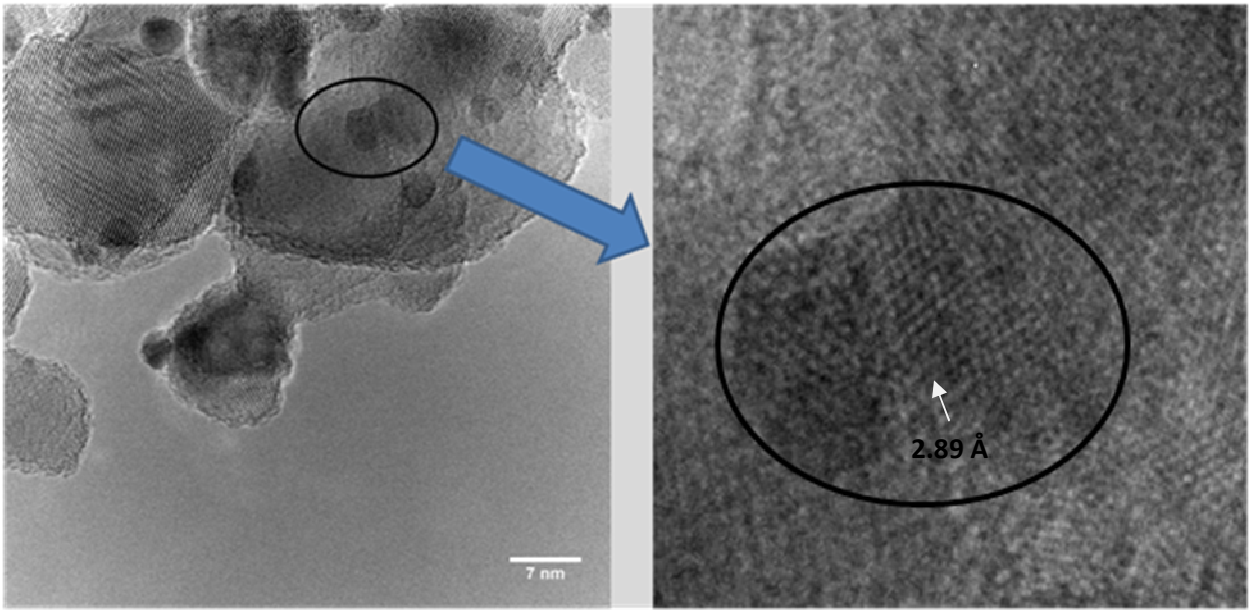

Figure 3.18: HRTEM image showing two particles forming one big particle. The white arrow showing the lattice distance of the lumpy particle on the zoomed area.

3.5 Conclusion

The synthesis conditions of Au/TiO_2 catalysts via the DP method are crucial. Based on the above findings pH, wt%, aging and calcination temperature are vital factors that affect deposition of small sized Au particles onto the support during synthesis. Particle size increased with increasing Au loading. Increasing pH of the solution during synthesis favoured deposition of small sized Au particles with pH 8 being optimum. The optimum calcination temperature was 200 °C. Particle size of Au particles decreased with increasing aging period with 72 h being the optimum aging period. Amorphous silica showed an increase in particle size making TiO_2 a better support for Au. The Au particles attached on the SiO_2 sintered indicating poor metal-support interaction.

Synthesis of Au-Pd catalysts via the DP method resulted in separately attached metals hence no alloy or core shell formed. Adsorption of separate metals was confirmed by the measured interatomic distances from the HRTEM images. However, Au or Pd could not be distinguished by colour or morphology from the TEM images. Pd particles could not be detected by XRD due to the low loading percentages. However, there was no increase in surface area indicating that the support was not entirely covered with the adsorbed metals. The change in pore volume confirmed that indeed the metals were adsorbed on the support.

3.6 References

[1] G.J. Hutchings, M. Haruta, *Appl. Catal. A*, 291 (**2005**) 2

[2] M. Haruta, *Gold Bull.*, 37 (**2004**) 27

[3] D. Astruc, F. L. Aranzaes, J. R. Angew, *Chem. Int. Ed*, 44 (**2005**) 7852

[4] M. Haruta, *CATTECH*, 6 (**2002)** 102

[5] M. Haruta, *Catal. Today*, 36 (**1997**) 153

[6] Y.A. Nechayev, G.V. Nikolenko, *Geochem. Int.*, 32 (**1986**) 23

[7] Haruta M, Daté M, *Appl. Catal. A*, 222 (**2001**) 427

[8] M. Kosmulski, *J. Colloid Interface Sci.*, 275 (**2004**) 214

[9] F. Moreau, G. C. Bond, A. O. Taylor, *J. Catal.*, 231 (**2005**) 105

[10] W.-C. Li, M. Comotti, F. Schüth, *J. Catal.*, 237 (**2006**) 190

[11] A. Wolf, F. Schüth, *Appl.Catal. A*, 226 (**2002**) 1

[12] R. Zanella, S. Giorgio, C.H. Shin, C. R. Henry, C. Louis, *J. Catal.*, 222 (**2004**) 357

[13] M. C. Raphulu, *PhD thesis*, University of the Witwatersrand, Johannesburg, **2004**

[14] A.Baiker, M. Maciejewski, S. Tagliaferri, P. Hug, *J. Catal.*, 151 (**1995**) 407

[15] W. F. Yan, B. Chen, S. M. Mahurin, V. Schwartz, D. R. Mullins, A. R. Lupini, S. J. Pennycook, S. Dai, S. H. Overbury, *J. Phys.Chem. B*, 109 (**2005**) 10676

[16] G. C. Bond, D. T. Thompson, *Gold Bull.*, 33 (**2000**) 41

[17] K. Tanaka, T. Akita, D.A.H. Cunningham, S. Tsobota, *Report of the Osaka National Research Institute*, 393 (**1999**) 11

[18] T. Minato, T. Susaki, S. Shiraki, H.S. Kato, M. Kawai, K. Aika, *Surf. Sci.*, 1012 (**2004**) 566

[19] S. K. Tanielyan, R. Augustine, *Appl. Catal. A*, 85 (**1992**) 73

[20] S.Inova, V. Pitchon, Y. Zimmermann, C. Petit, Appl. *Catal. A*, 298 (**2006**) 57

[21] M. Haruta, H.Sano, T. Kobayasi, *US Patent*, 4698324 (**1987**) 405

[22] M. Haruta, *Catal. Surveys Japan*, 1 (**1997**) 61

[23] Y.J. Chen, C. T. Yeh, *J. Catal.*, 200 (**2001**) 59

[29] M. Date´, Y. Ichihashi, T. Yamashita, A. Chiorino, F. Boccuzzi, M. Haruta, *Catal. Today*, 72 (**2002**) 89

[24] J. –N, Lin, B. –Z, Wan, *Appl. Catal. B*, 41 (**2003**) 83

[25] N. D. Tran, M.` le Besson, C. Descorme, *J. Chem*, 35 (**2011**) 2095

[26] U. Landman, *Proc. Natl. Acad. Sci. USA*, 102 (**2005**) 6671

[27] K. Asakura, Y. Iwasawa, A. I. Kozlova, H. Liu, T. Shido, *J. Catal*., 185 (**1999**) 252

[28] D. Wang, Y. Li, *Adv. Mater*, 23 (**2011**) 1044

[29] D.A.H Cunningham, M. Haruta, W.Vogel, H. Kagayama, S. Tsubota, *J. Catal.*, 177 (**1998**) 1

[30] M. Comotti, W. C. Li, B. Spliethoff, F. Schuth, *J. Am. Chem. Soc*., 128 (**2006**) 917

[31] S. C. Parker, A. W. Grant, V. A. Bondzie, C. T. Campbell, *Surf. Sci*., 441 (**1999**) 10

[32] S. H. Overbury, L. Ortiz-Soto, H. Zhu, B. Lee, M. D. Amiridis, S.Dai, *Catal. Lett.*, 95 (**2004**) 99

[33] H. Z. Zhu, B. Lee, S. Dai, S. H. Overbury, *Langmuir*, 19 (**2003**) 3974

[34] V. A. Bondzie, S. C. Parker, C. T. Campbell, *Catal. Lett*, 63 (**1999**) 143

[35] Z. Ma, F. Zaera, *Heterogeneous Catalysis by Metals*, R. B. King (Ed.), Encyclopedia of Inorganic Chemistry,2nd edition, Wiley, Chichester, (**2005**) 1768

[36] W. F. Yan, B. Chen, S. M. Mahurin, E. W. Hagaman, S. Dai, S. H. Overbury, *J. Phys. Chem. B*, 108 (**2004**) 2793

[37] H. Huber, D. McIntosh, G. A. Ozin, *Inorg. Chem*, 16 (**1997**) 975

[38] N. Lopez, J. K. Nørskov, T. V. W. Janssens, A. Carlsson, A. Puig-Molina, B. S. Clausen J.-D. Grunwaldt, *J. Catal*., 225 (**2004**) 86

[39] J.-D. Grunwaldt, C. Kiener, C. Wo¨gerbauer, A. J. Baiker, *J. Catal.*, 181 (**1999**) 223

[40] J. K. Edwards, A. F. Carley, A. A. Herzing, C. J. Kiely, G. J. Hutchings, *Faraday Discuss*, 138 (**2008**) 225

[41] M. S. Chen, D. Kumar, C. W. Yi, D. W. Goodman, *Science*, 310 (**2005**) 291

[42] S. Marx, A. J. Baiker, *Phys. Chem. C*, 113 (**2009**) 6191

[43] M. Conte, A. F. Carley, G. Attard, A. A. Herzing, C. J. Kiely, G. J. Hutchings, *J. Catal.*, 257 (**2008**) 190

[44] D.I. Enache, J. K. Edwards, P. Landon, B. Solsona-Espriu, A. F. Carley, A. A. Herzing, M. Watanabe, C. J. Kiely, D. W. Knight, G. J. Hutchings, *Science*, 311 (**2006**) 362

[45] W. C. Ketchie, M. Murayama, R. J. Davis, *J. Catal.*, 250 (**2007**) 264

[46] P. Landon, P. J. Collier, A. F. Carley, D. Chadwick, A. J. Papworth, A. Burrows, C. J. Kiely, G. J. Hutchings, *Phys. Chem*, 5 (**2003**) 1917

[47] L. Guczi, *Catal. Today*, 53 (**2005**) 101

[48] A. E. Hahelin-Weaver, J. F. Weaver, G. B. Hoflund, G. N. Salaita, *J. Alloys Comp*, 393 (**2005**) 93

[49] Y. Robach, M. Abel, L. Porte, *Surf. Sci*, 526 (**2003**) 248

[50] L. Prati, M. Rossi, *J. Cata.*, 176 (**1998**) 552

[51] J. Schwank, *Gold Bull.*, 2 (**1985**) 18

[52] J. K. Edwards, B. Solsona-Espriu, P. Landon, A. F. Carley, A. A. Herzing, C. J. Kiely, G.J. Hutchings, *J. Catal.*, 236 (**2005**) 69

[53] K. Gschneidner , A. Russell, A. Pecharsky, J. Morris, Z. H. Zhang, T. Lograsso, D. Hsu, C. H. C. Lo, Y. Y. Ye, A. Slager, D. Kesse , *Nature Mater*, 2 (**2003**) 587

[54] L. Prati, A. Villa, F. Porta, D. Wang, D. Su, *Catal. Today*, 122 (**2007**) 386

[55] B. B. Lim, M. Jiang, J. Tao, P. H. C. Camango, Y.Zhu, Y. Xia, *Adv. Funct. Mater*, 19 (**2009**) 189

[56] F. Liu, D. Wechsler, P. Zhang, *Chem. Phys. Let.*, 461 (**2008**) 254

[57] T. Shibata, H. Tostmann, B. Bunker, A. Henglein, D. Meisel, S. Cheong, M. J. Boyanov, *Synchrotron Rad*, 8 (**2001**) 545

[58] P. Dash, T. Bond, C. Fowler, W. Hou, N. Coombs, R. W. J. Scott, *J. Phys. Chem. C* 113 (**2009**) 12719

[59] H. Ohnishi, Y. Kondo, K. Takayanagi, *Nature*, 395 (**1998**) 780

[60] V. Rodrigues , D. Ugarte, *Phys. Rev. B*, 63 (**2002**) 73405